

# Iron Aluminides

Martin Palm, Frank Stein, and Gerhard Dehm

Department of Structure and Nano/Micromechanics of Materials, Max-Planck-Institut für Eisenforschung GmbH, D-40237 Düsseldorf, Germany; email: m.palm@mpie.de, f.stein@mpie.de

Annu. Rev. Mater. Res. 2019.49:297-326. Downloaded from www.annualreviews.org. Access provided by WIB60417 - Max-Planck-Gesellschaft on 12/16/20. For personal use only.

Annu. Rev. Mater. Res. 2019. 49:297–26

First published as a Review in Advance on March 27, 2019

The *Annual Review of Materials Research* is online at [matsci.annualreviews.org](http://matsci.annualreviews.org)

<https://doi.org/10.1146/annurev-matsci-070218-125911>

Copyright © 2019 by Annual Reviews. All rights reserved

## Keywords

iron aluminides, intermetallics, mechanical properties, corrosion, processing, physical properties

## Abstract

The iron aluminides discussed here are Fe–Al-based alloys, in which the matrix consists of the disordered bcc (Fe,Al) solid solution (A2) or the ordered intermetallic phases FeAl (B2) and Fe<sub>3</sub>Al (D0<sub>3</sub>). These alloys possess outstanding corrosion resistance and high wear resistance and are lightweight materials relative to steels and nickel-based superalloys. These materials are evoking new interest for industrial applications because they are an economic alternative to other materials, and substantial progress in strengthening these alloys at high temperatures has recently been achieved by applying new alloy concepts. Research on iron aluminides started more than a century ago and has led to many fundamental findings. This article summarizes the current knowledge of this field in continuation of previous reviews.

**ANNUAL REVIEWS CONNECT**

[www.annualreviews.org](http://www.annualreviews.org)

- Download figures
- Navigate cited references
- Keyword search
- Explore related articles
- Share via email or social media

## 1. HISTORICAL REMARKS

Iron and aluminum are the most abundant metals in the earth's crust. Therefore, it is not surprising that, more than a century ago, metallurgists became interested in producing useful alloys from these elements. The first discovery was that iron resists oxidation if alloyed with aluminum (1, 2). It also became apparent that the wear resistance of Fe increased by alloying with Al, although at the expense of ductility (3). In the first decades of the twentieth century, the search for alloys with sufficient strength at high temperatures, i.e., above 600°C, and an acceptable minimum of ductility at ambient temperatures dominated the development of Fe–Al-based alloys. Early developments in Russia and Britain led to patented alloys (4–7), which had already been tested and optimized for various properties. However, published evidence of these developments is scarce. The first major development from which commercial parts were produced to some extent was Pyroferal<sup>®</sup>, an Fe–Al–C-based alloy, which was developed in the early 1950s in the former Czechoslovakia (8–11). It was reportedly invented when scrap from World War II army remains was melted down to overcome a shortage in raw materials. As the scrap contained a high share of airplane wreckage, the resulting alloys had a high Al content. Compositions were optimized, and the resulting alloys were employed for sand castings of heat-resistant equipment for furnaces. The precise composition of Pyroferal has not been preserved, but it must have been approximately Fe–45Al–3.5C (11). Production ceased in the early 1960s, when alloying elements for the production of stainless steels became available again. However, there was an additional, more apparent, reason: Parts cast from Pyroferal repeatedly disintegrated to powders after casting or while they were awaiting shipment in the company's outside yard (12). It is now clear that the compositions of Pyroferal were quite close to the three-phase equilibrium  $B2\text{FeAl} + \text{graphite} + \text{Al}_4\text{C}_3$ . As  $\text{Al}_4\text{C}_3$  disintegrates in contact with hydrogen, e.g., in moist air, such reports seem plausible.

Developments of Fe–Al-based alloys in the United States can be traced back to at least the early 1950s, when alloy series termed Alfenol and Thermenol were developed at the Naval Ordnance Laboratory (13–16), Ferral at the Ford Motor Company (17–19), DB-2 at The Martin Company (20, 21), and Fe–Cr–Al at the Batelle Memorial Institute (22). Prototype duct halves and jet engine compressor blades were forged from these alloys, and furnace hearths, heat-treat boxes, and turbine exhaust cones were welded (13, 15, 16, 23, 24). Reports from the Batelle Memorial Institute provide an excellent summary of the early developments in the United States (25, 26). The development of Alfenol and specifically of Thermenol continued until the early 1970s under a contract with the US Office of Saline Water in search of corrosion-resistant tubes for use in seawater desalination (27). The feasibility of using Fe–Al in aircraft engines was investigated through the 1980s by Pratt & Whitney and TRW Inc. under contracts with the Air Force Wright Aeronautical Laboratories (28, 29). Finally, starting in the late 1980s, alloys based on  $\text{D0}_3\text{Fe}_3\text{Al}$  and B2 FeAl were investigated in detail at the Oak Ridge National Laboratory (ORNL) in programs aimed at developing new materials for fossil fuel conversion (30). Specifically, this extensive work at ORNL and collaborating institutions led to a more in-depth understanding of iron aluminide-based alloys. In particular, the phenomenon of environmental embrittlement (31) and details of the yield stress anomaly (YSA) were encountered and clarified. Most of the ORNL reports are now available and are an invaluable resource on all aspects of properties, alloy developments, and processing of iron aluminide-based alloys, and a number of reviews summarize the work (32–36).

Efforts to note in other countries include research in India, France—where the oxide dispersion-strengthened (ODS) Grade 3 alloy was developed (37, 38)—Germany, and the Czech Republic, as well as research by Maria Muñoz-Morris and David Morris at the University of Neuchâtel, Switzerland, and later at CENIM in Madrid, Spain (39, 40).

These efforts have been motivated by the advantageous properties of the iron aluminides, such as their outstanding corrosion and wear resistance and relatively low density, as well as by the economic advantages of replacing stainless steels or Ni-base superalloys. The current review provides an overview of the basic properties, physical metallurgy, processing, and applications of Fe–Al-based alloys, especially the past 25 years, in continuation of previous reviews (32, 41, 42).

## 2. PHASE DIAGRAM AND CRYSTAL STRUCTURES

The current review focuses on Fe–Al-based alloys with Al contents of up to approximately 50 at%. **Figure 1a** shows the phase diagram of the binary system in this composition range, revealing a very high solubility of Al in the bcc  $\alpha$ Fe (A2) solid solution (43). Depending on the temperature, up to 45-at% Al can be dissolved in the disordered bcc (Fe,Al) solid solution, which is usually denoted by its Strukturbericht symbol, A2. While the added Al atoms statistically replace Fe atoms in the disordered A2 phase, two different types of ordering of the Al atoms on the bcc lattice sites occur at higher Al contents. For the B2-ordered phase FeAl, the corners of the cubic unit cell are completely occupied by Fe atoms, while Al atoms are located at the center positions. The lattice of the D0<sub>3</sub>-ordered phase Fe<sub>3</sub>Al is also based on the simple bcc unit cell. However, in this case the ideal structure is formed from cells with periodically alternating Al or Fe atoms in the center of the cubic cell (see **Figure 1b**), and the resulting D0<sub>3</sub> structure has an fcc lattice.

Many publications state that the investigated alloys are Fe<sub>3</sub>Al based or FeAl based. These denominations usually refer to Al contents between (a) approximately 25 and 35 at% and (b) approximately 35 and 52 at%, respectively. However, as **Figure 1** shows, Fe<sub>3</sub>Al-based alloys will become

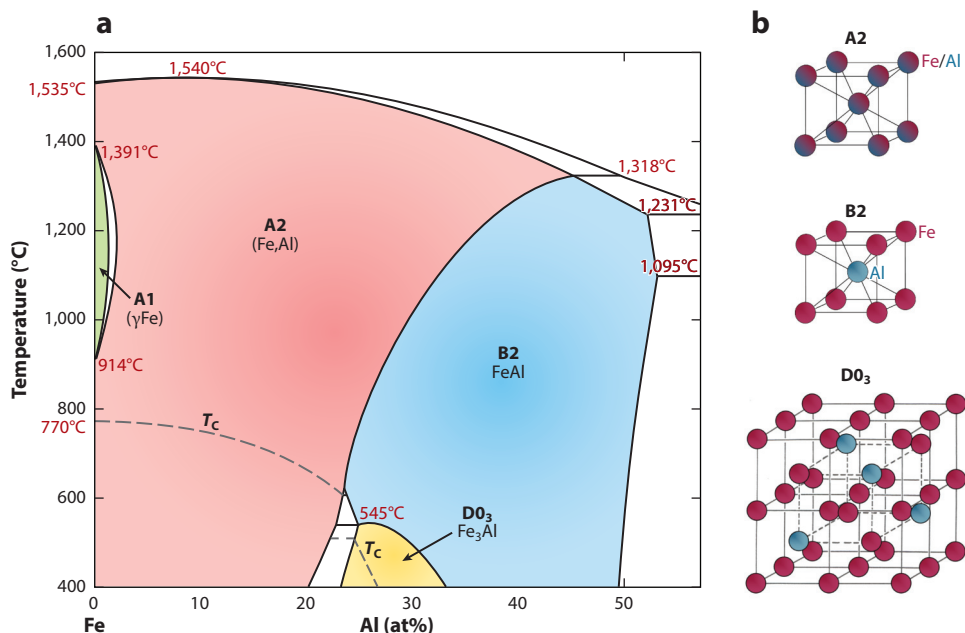


**Figure 1**

(a) The Fe-rich part of the Fe–Al phase diagram showing the extended phase fields of the A2-disordered solid solution (Fe,Al), B2-ordered solid solution (FeAl), and D0<sub>3</sub>-ordered solid solution (Fe<sub>3</sub>Al).  $T_c$  is the ferromagnetic Curie temperature. Panel a is based on data reported in Reference 43. (b) The unit cells of the three cubic structures (Fe, red; Al, blue; Fe or Al, shaded violet).

B2-ordered FeAl or even disordered A2 (Fe,Al) and FeAl-based alloys will become disordered A2 (Fe,Al) with increasing temperature.

### 3. SELECTED PHYSICAL PROPERTIES

The physical properties of Fe–Al alloys are strongly affected by Al content and ordering state. Out of the vast amount of literature on this topic, here we give only a few examples, focusing on some selected, mainly application-related properties.

#### 3.1. Density, Lattice Parameters, and Thermal Expansion

Al is lighter than Fe, and Al atoms are larger than Fe atoms. These two factors contribute to the very beneficial, weight-reducing effect of Fe–Al-based materials as the density decreases from 7.87 g/cm<sup>3</sup> for pure Fe to 5.59 g/cm<sup>3</sup> for Fe-50Al (44). While the lattice parameter of the disordered A2 (Fe,Al) solid solution increases approximately linearly with Al content, the onset of D0<sub>3</sub> or B2 ordering leads to a significant decrease in the lattice parameter relative to the disordered A2 state (45). The thermal expansion coefficients increase with Al content but are sensitive to changes in ordering and magnetic state (46–48).

#### 3.2. Young's Modulus

The Young's modulus of the A2 (Fe,Al) solid solution is strongly reduced by adding Al. The room-temperature values continuously decrease from 210 GPa for pure Fe to a minimum of 121 GPa near 26-at% Al in D0<sub>3</sub> Fe<sub>3</sub>Al and then increase to 173 GPa at 36-at% Al. Above this composition in B2 FeAl, the room-temperature Young's modulus remains approximately constant up to 50-at% Al (49).

#### 3.3. Diffusivity and Thermal Conductivity

Tracer diffusion experiments show that the diffusivities of Fe and Al are of a similar magnitude in Fe–Al alloys (50). The activation enthalpy for diffusion of Fe in Fe–Al alloys increases with increasing order as well as with increasing Al content. A comparison between the activation enthalpies of diffusion and defect formation and migration enthalpies suggests that diffusion is mediated by vacancy-type defects (50, 51).

The thermal conductivity of iron aluminides is poorer than that of stainless steels. With respect to composition, both the room-temperature thermal conductivity and diffusivity reach local maxima at the stoichiometric compositions of the ordered compounds D0<sub>3</sub> Fe<sub>3</sub>Al and B2 FeAl while decreasing at intermediate compositions to minimum values of 9.5 W/(m·K) and 2.8·10<sup>-6</sup> m<sup>2</sup>/s at 34-at% Al (52). Rudajevová & Buriánek (52) report that the thermal diffusivity is affected not only by ordering but also by the presence of ferromagnetism, leading to a complex dependence on temperature. In contrast, the thermal conductivity continuously increases with temperature for all compositions.

#### 3.4. Electrical Properties

As expected, the electrical resistivity of the A2 (Fe,Al) solid solution increases upon alloying with Al at room temperature. Interestingly, it reaches a sharp maximum at 33–34-at% Al in D0<sub>3</sub> Fe<sub>3</sub>Al and decreases again on further Al addition up to 50 at% (53). This experimentally observed anomaly

in the electrical resistivity occurs independently of heat treatment and ordering state (53) and was explained to be a direct consequence of a continuous change in the electronic structure due to the filling of the Fe *3d* bands with Al *3p* valence electrons (54).

### 3.5. Magnetic Properties

At room temperature, Fe–Al is ferromagnetic up to an Al content of approximately 32 at%. The ferromagnetic Curie temperature  $T_C$  of the A2 (Fe,Al) solid solution decreases from 770°C for pure Fe to 600°C at 23-at% Al, and  $T_C$  of D0<sub>3</sub> Fe<sub>3</sub>Al decreases from 508°C at 24-at% Al to –273.2°C (0 K) at approximately 32-at% Al (43, 55). The average magnetic moment per atom decreases upon alloying with the nonmagnetic Al. In the disordered A2 state, the amount of the reduction can be described well by a simple dilution model, while the occurrence of D0<sub>3</sub> ordering results in a significantly stronger decrease in the moment per atom. B2 FeAl is not ferromagnetic because, due to the high Al content and the B2 ordering, the number of Fe nearest-neighbor atoms surrounding an Fe atom is no longer sufficient to produce a ferromagnetic moment. However, by introducing some disorder into a B2 FeAl alloy, regions in the lattice can be produced with sufficient Fe nearest neighbors to result in some spontaneous magnetization. Indeed, experiments proved that disordering of B2 Fe–40Al by ball milling (56), cold rolling (57), ion irradiation (58, 59), or laser irradiation (60) leads to ferromagnetism. As this effect of disorder-induced ferromagnetism is reversible and the material can be transformed back to the paramagnetic state by annealing, there were attempts to use the ion irradiation technique for small-scale magnetic patterning, i.e., for fabricating arrays of submicrometer ferromagnetic structures at the surface of nonmagnetic intermetallic Fe–40Al sheets, either via the focused ion beam (FIB) technique or via ion irradiation through prelithographed PMMA [poly(methyl methacrylate)] masks (58, 59). However, both methods have shortcomings. While FIB is a rather slow patterning technique, writing the dots one by one, irradiation through PMMA masks leads to a progressive thinning of the masks until the remaining PMMA layer is too thin to stop the incoming ions (59). More recently, short-pulse laser irradiation applied to polycrystalline B2 Fe–40Al films was successfully proven to be another method for producing rewritable ferromagnetism (60).

## 4. MECHANICAL PROPERTIES

### 4.1. Yield Strength

Iron aluminide-based alloys possess excellent yield strength in relation to steels and Co- and Ni-base alloys (see **Figure 2a**). Particularly if the density-corrected specific strength (**Figure 2b**) is considered, iron aluminides have the potential to replace these more expensive materials, at least for temperatures of up to 800°C.

A closer look at the temperature dependence of the yield stress of iron aluminide-based alloys reveals that three different ranges exist (**Figure 3**). For temperatures of up to approximately 400°C, the yield strength is strongly influenced by quenched-in vacancies; i.e., the processing of the material plays a crucial role. Fe–Al alloys contain a comparable high amount of thermal vacancies, which at lower temperatures strongly affect the mobility of dislocations. The high number of constitutional vacancies is due to their low enthalpy of formation [ $H_v^f = 0.7\text{--}1.2$  eV for D0<sub>3</sub> Fe<sub>3</sub>Al (61–63);  $H_v^f = 0.8\text{--}1.1$  eV for B2 FeAl (62, 64, 65)]. Depending on the vacancy concentration, the yield stress can vary by a factor of two to five for a given composition (66, 67). Therefore, for comparison of the yield stress of different Fe–Al alloys, usually a heat treatment at 400°C for 168 h is performed because a minimum concentration of thermal vacancies can be obtained at approximately this temperature (68, 69). However, for Fe–Al alloys envisioned for service at ambient

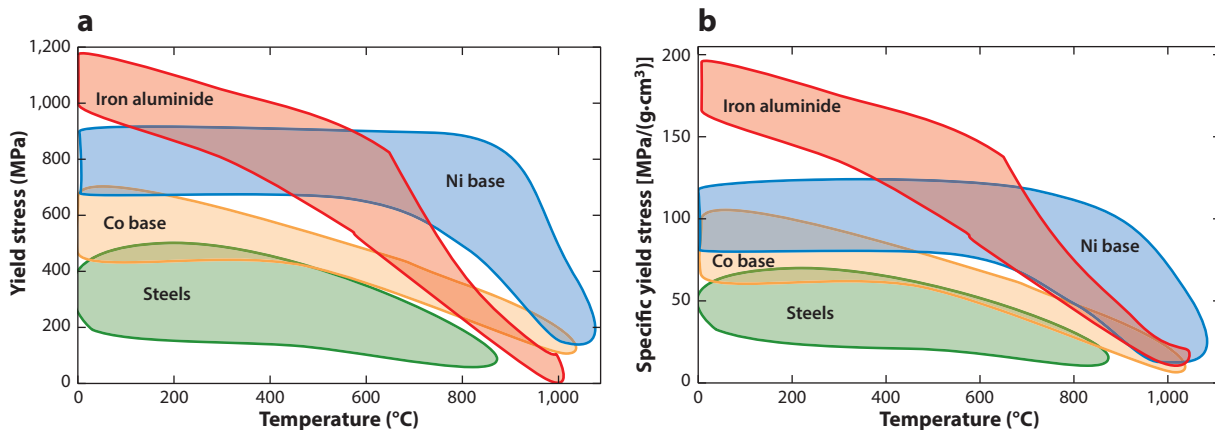


**Figure 2**

(a) Yield strength and (b) density-corrected specific yield strength of iron aluminide-based alloys in relation to steels and Co- and Ni-base alloys at  $\dot{\epsilon} = 10^{-4} \text{ s}^{-1}$ .

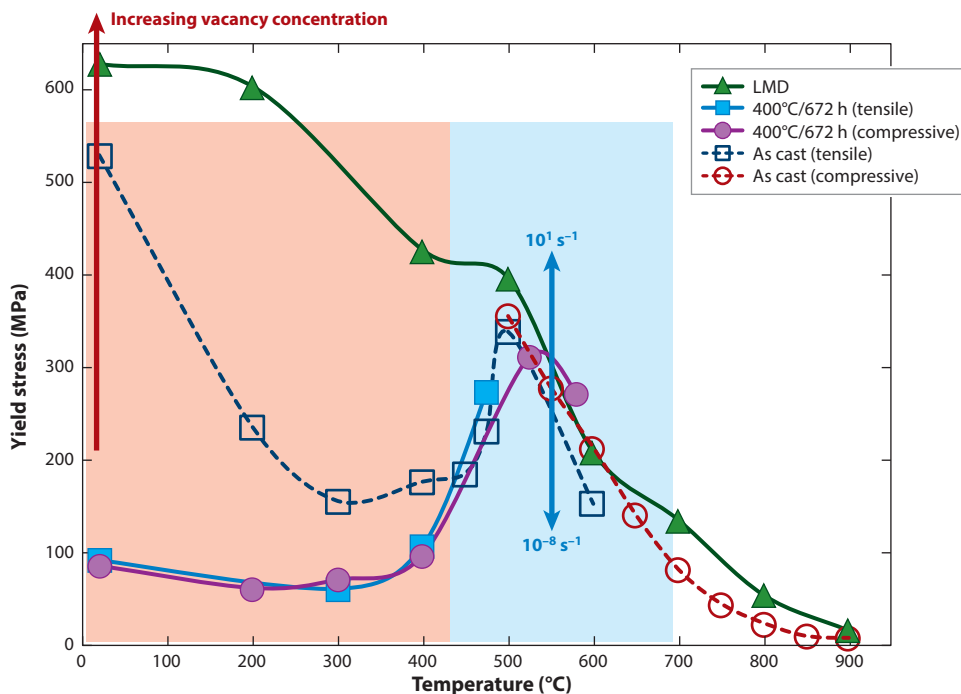


**Figure 3**

$\sigma_{0.2}$  tensile or compressive yield stress of Fe–26–28-at% Al after rapid cooling [laser metal deposition (LMD)], after moderate cooling (as cast), and in a well-annealed state (400°C/672 h). The strain rate is  $1 \times 10^{-4} \text{ s}^{-1}$ . The area shaded in red indicates the temperature range in which the yield stress is influenced by quenched-in vacancies, and the red arrow indicates how the yield stress varies with vacancy concentration. The area shaded in blue shows the temperature range in which the yield stress is affected by the yield stress anomaly (YSA), and the blue arrow indicates the dependence of the YSA on deformation rate. Previously unpublished data of as-cast and annealed alloys are from J. Deges. LMD data are from Reference 126.

temperatures, strengthening by quenched-in (i.e., thermal) vacancies is a viable method, and the yield stress may be adjusted by controlling the cooling rate.

Between approximately 400°C and 600°C, iron aluminide-based alloys show an increase in yield stress (**Figure 3**). This unusual increase with increasing temperature, termed YSA, is observed for many intermetallic phases. It has been conclusively shown that the YSA in Fe–Al is not connected with the  $D0_3 \leftrightarrow B2$  transformation (70). Although the underlying mechanisms have not been fully clarified, quenched-in vacancies clearly play a major role (40, 71–74). Up- and down-quenching experiments after various heat treatments (73, 75) led to the conclusion that hardening by immobile thermal vacancies on the low-temperature side of the YSA and loss of hardening due to increased thermal mobility with increasing temperature are responsible for the YSA (72). In addition, a change in the dislocation structure for B2 from  $\langle 111 \rangle$  superdislocations to  $\langle 100 \rangle$  perfect dislocations (76–79) occurs in the temperature range of the YSA. Reactions or decomposition of the  $\langle 111 \rangle$  superdislocations creating local pinning points (39, 80), combined with quenched-in vacancies, is believed to contribute to the YSA (40, 81). Such mechanisms explain the strong strain rate dependence of the yield stress in the range of the YSA. Although one investigation found only a minor decrease in the peak of the YSA at decreasing strain rates (82), the general observation is that a pronounced decrease in the peak of the YSA occurs with decreasing strain rates, which may lead to the vanishing of the YSA peak at strain rates below  $1 \times 10^{-7} \text{ s}^{-1}$  (74, 83, 84). The practical consequences are that, under the low strain rate deformation conditions often seen in service at high temperatures, i.e., creep, the YSA has no strengthening effect, while at high deformation rates, e.g., during hot forming in this temperature range, unduly high strength may be encountered. The temperature at which the actual maximum of the YSA occurs and the actual yield stress at the YSA can be widely affected by alloying, and even twofold YSAs have been reported (85).

Above the YSA peak temperature, Fe–Al alloys show normal behavior in that the yield stress decreases with increasing temperature. This decrease is particularly rapid in binary Fe–Al alloys (**Figure 4**). Because this problem has long been considered the major obstacle in the application of Fe–Al alloys, extensive efforts have been devoted to increasing the strength at high temperatures (39, 86–90). Section 4.3 provides an overview of different strengthening strategies.

The yield stress of binary Fe–Al between room temperature and 550°C increases with increasing Al content up to a pronounced maximum just below 25-at% Al, i.e., the stoichiometric composition of  $\text{Fe}_3\text{Al}$  (**Figure 4**). After a sharp drop, the yield stress rises again with further increases in Al content (32, 91–93). With increasing temperature, the maximum becomes less pronounced, and at 700°C, i.e., above the stability of  $D0_3 \text{ Fe}_3\text{Al}$  in the binary system, only a slight increase in the yield stress with Al content and the absence of a maximum are observed (92). Additionally, no marked increase in the yield stress is observed at this temperature when the disordered A2 (Fe,Al) solid solution becomes ordered B2 FeAl at higher Al contents (**Figure 4**).

## 4.2. Creep

One of the early key findings was that binary Fe–Al alloys lose their (creep) strength near the critical temperature of the  $D0_3/B2$  transition (94). The decrease in long-range order, which leads to a higher mobility of the dislocations, is the obvious explanation. However, as Cahn (95) pointed out, interdiffusion in B2 FeAl has a pronounced composition dependence. Therefore, a decrease in interdiffusivity or a lowered self-diffusion in  $D0_3 \text{ Fe}_3\text{Al}$  relative to B2 FeAl may also account for the higher creep resistance of  $D0_3 \text{ Fe}_3\text{Al}$  (95). Creep in B2 FeAl is controlled by viscous glide of dislocations not leading to subgrain formation, and a high dislocation density therefore results. This results in low stress exponents between 3 and 4 (96). By alloying, the deformation behavior

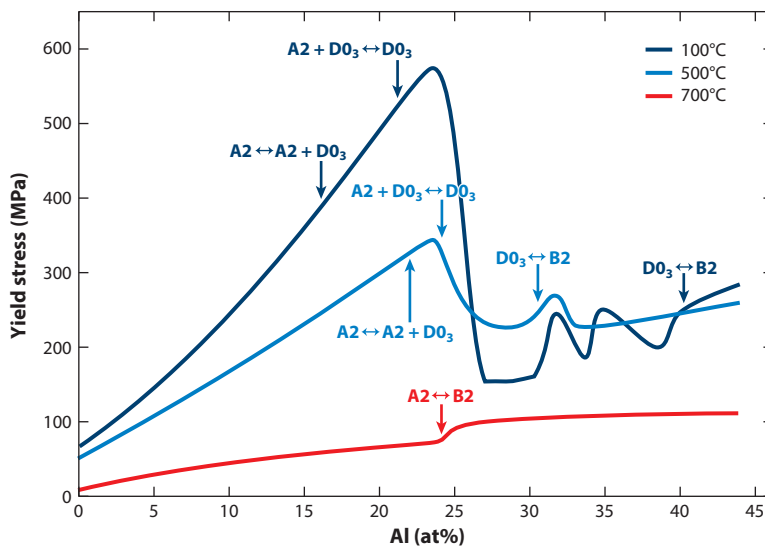


**Figure 4**

$\sigma_{0.2}$  yield stress of binary Fe–Al at 100°C, 500°C, and 700°C as a function of Al content (based on data from References 70, 92, and 293–295) for strain rates of  $1 \times 10^{-4} \text{ s}^{-1}$  to  $3 \times 10^{-3} \text{ s}^{-1}$ . Compositions indicated by arrows for the A2/B2/D0<sub>3</sub> transition at the temperatures shown are from Reference 43, with data for 100°C extrapolated from higher temperatures.

during creep can be changed to be controlled by dislocation climb. In this case, stress exponents between 4 and 5 are observed, and these values are typical for many iron aluminide alloys (96). Also, creep strength is little—if at all—affected by the Al content (74), while at least for Al-rich B2 FeAl, the initial grain size has a marked, if complex, effect (97). In summary, creep strength of binary Fe–Al is inadequate due to the high diffusivity in the open bcc lattice (74).

### 4.3. Alloying Concepts for Enhanced (Creep) Strength

Insufficient creep strength above approximately 500°C has been a major concern that has prohibited a wider application of iron aluminide-based alloys. Classical strengthening concepts for Fe–Al alloys are derived from the developments of steels and rely mainly on carbide precipitation. Although an appreciable increase in (creep) strength can be achieved, strength usually falls short relative to advanced high-alloyed steels, e.g., P92 (**Figure 5**). Moreover, (a) carbides tend to coarsen rapidly above a threshold temperature, resulting in a drastic drop in strength; (b) an even distribution of fine carbide precipitates, specifically at grain boundaries, is hard to attain; and (c) most carbides form plates or needles, acting as internal sources for crack nucleation within the brittle material.

Borides have approximately the same strengthening effect as carbides (**Figure 5**). However, as they often form by a eutectic reaction and not from a supersaturated solid solution, alignment of the boride precipitates along grain boundaries is possible. Such a distribution of the boride precipitates is important, as one reason for the loss of strength at high temperatures is the rapid coarsening of the Fe–Al matrix. The borides pin the grain boundaries and do not coarsen up to high temperatures (98, 99). Furthermore, boride-strengthened alloys have improved ductility (see Section 4.4).

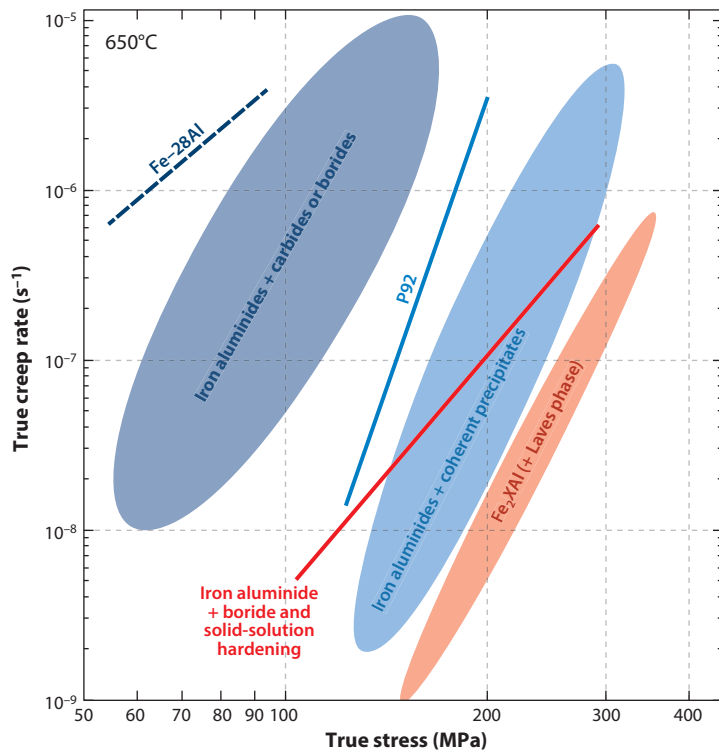


**Figure 5**

Secondary creep of iron aluminide-based alloys (at 650°C) strengthened by different mechanisms. Data for binary Fe–28Al (from Reference 296) and the high-strength 9-wt% Cr steel P92 (from Reference 297) are shown for comparison. Other data from References 116, 120, and 298.

Fe–Al alloys with coherent precipitates—also termed ferritic superalloys, as their microstructures resemble those of Ni-base superalloys—have (creep) strengths that often outperform those of advanced steels (**Figure 5**) (100). With respect to strengthening, whether the alloys have an A2 + B2, an A2 + L2<sub>1</sub>, or a B2 + L2<sub>1</sub> microstructure does not matter. Coherent microstructures can form where a stable miscibility gap exists (e.g., Fe–Al–X systems, with X = Ni, Co, V, Ti) or metastably during cooling when precipitation of the stable (Laves) phase in the supersaturated matrix is kinetically retarded (X = Nb, Ta). While for the former alloys rapid coarsening can be an issue, the latter ones are limited in temperature in that the stable Laves phase forms in Fe–Al–Nb above approximately 650°C (101) and in Fe–Al–Ta above 750°C (102). In principle, the Laves phase can also be employed for the strengthening of Fe–Al alloys, but again the uncontrollable distribution, specifically when the Laves phase solidifies from the melt, has precluded any alloy developments.

However, the abovementioned transformation from the metastable Heusler phase to the stable Laves phase can help to control the distribution of the Laves phase within the microstructure. By long-term heat treatments, doping with boron or hot working and a successive short heat treatment precipitation of the Laves phase at grain or subgrain boundaries can be realized (103, 104). Such strengthening by thin films of intermetallic phases, e.g., the Laves phase, on grain boundaries is also a new concept currently being investigated for steels (105, 106).

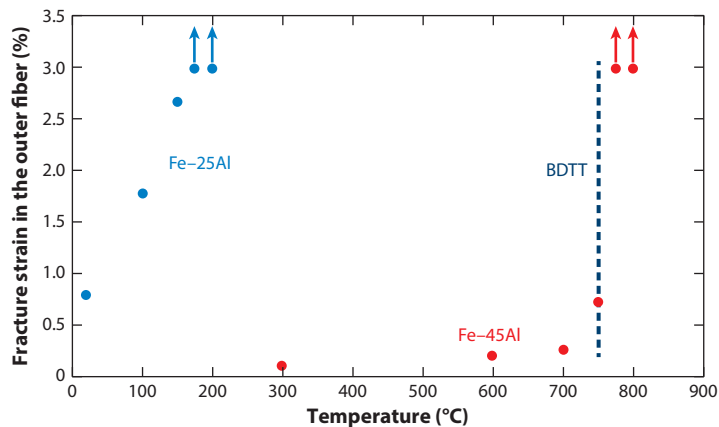


**Figure 6**

Transition from brittle to ductile behavior in Fe–25Al (continuous) and Fe–45Al (abrupt) with marked brittle-to-ductile transition temperature (BDTT). Data from Reference 115.

Binary Fe–Al alloys lose their strength when the fcc  $D0_3$  structure transforms to B2 with increasing temperature. As the maximum temperature for this transformation is  $545^\circ\text{C}$ , increasing this transformation temperature through alloying is another viable approach for strengthening Fe–Al alloys. In some Fe–Al– $X$  systems, complete miscibility exists between binary  $D0_3$  and the ternary structural equivalent  $L2_1$  up to the composition of the Heusler phase  $\text{Fe}_2\text{XAl}$ . With increasing  $X$  content, the  $D0_3$  ( $L2_1$ )/B2 ordering temperature increases, e.g., to more than  $1,025^\circ\text{C}$  for  $\text{Fe}_2\text{VAl}$  (107) and up to  $1,212^\circ\text{C}$  for  $\text{Fe}_2\text{TiAl}$  (108). The resulting alloys are strong (**Figure 5**) (107) but are also usually quite brittle (109).

As  $D0_3$   $\text{Fe}_3\text{Al}$  and B2 FeAl have large solid solubilities for many alloying elements, solid-solution hardening is a viable method for increasing the yield stress. For example, the  $800^\circ\text{C}$  yield stress of B2 FeAl can be increased from approximately 20 MPa to 90–115 MPa by alloying with 4-at% V, Ti, or Mo (90). Therefore, solid-solution hardening of the Fe–Al matrix can be used as an additional measure for strengthening. In addition, the alloying elements may raise the  $D0_3 \leftrightarrow \text{B2}$  transition temperature. Combined with boride strengthening, Fe–Al alloys such as Fe–Al–Mo–Ti–B may thus attain a modest strength at higher temperatures, as shown in **Figure 5**.

#### 4.4. Ductility

Although intrinsically ductile, both  $D0_3$   $\text{Fe}_3\text{Al}$  and B2 FeAl are subject to moisture or hydrogen embrittlement (110, 111), which is a concern for nearly every practical application. Environmental embrittlement is related to hydrogen interacting with the crack tip. The iron aluminide reacts with moisture, forming  $\text{Al}_2\text{O}_3$  and atomic hydrogen (31, 110). The hydrogen propagates to the crack tip, causing brittle cleavage crack propagation and premature failure (111). Therefore, tensile ductility at room temperature does not exceed 2–4% in the presence of moisture (42), which however is still favorable relative to many other intermetallic phases. Zamanzade et al. (112) provided a detailed review of hydrogen embrittlement of iron aluminides.

Interestingly, binary  $D0_3$   $\text{Fe}_3\text{Al}$  and B2 FeAl do not show a marked brittle-to-ductile transition temperature (BDTT) up to approximately 42-at% Al; marked BDTT is a characteristic feature of most intermetallic phases (96, 113, 114). Instead, the change from brittle to ductile behavior takes place gradually over a temperature range of  $150\text{--}200^\circ\text{C}$  (**Figure 6**). Also, relative to other

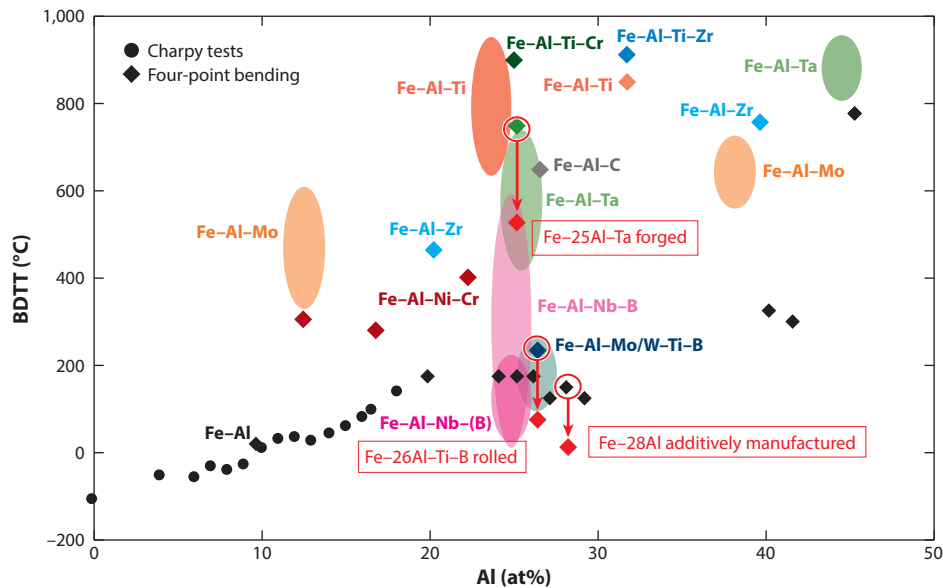


**Figure 7**

Brittle-to-ductile transition temperatures (BDTTs) of as-cast Fe-Al(*X*...) alloys. Increased ductility after processing is denoted by arrows. Data for binary Fe-Al from Reference 294 (Charpy tests) and Reference 115 (four-point bending). Figure adapted with permission from Reference 116.

intermetallic phases, binary Fe-Al alloys are ductile at relatively low temperatures. Up to approximately 42-at% Al, they become ductile between  $-100^{\circ}\text{C}$  (0-at% Al) and  $100^{\circ}\text{C}$ , while the temperature at which the alloy becomes ductile jumps to  $750^{\circ}\text{C}$  (115, 116). This jump is associated with a change from transgranular to intergranular fracture, and the alloys then show a clear BDTT (Figure 6). Unfortunately, nearly all Fe-Al-*X* alloys show a comparable jump in that only small additions of a third element drastically increase the temperature at which the alloy becomes ductile (Figure 7).

Increasing the ductility of iron aluminide alloys has been another major research topic. As the brittleness of the Fe-Al alloys is due to environmental effects, alloying may be beneficial. However, of all investigated additions, Cr is the only one that may improve ductility by having a direct effect on environmental embrittlement, although reports are varying. Zamanzade et al. (112) provided a comprehensive review, with specific emphasis on the effect of Cr. Small additions of boron have also been claimed to increase the ductility of B2 FeAl (42, 89, 117), possibly because boron segregates to grain boundaries, thereby increasing grain boundary cohesion (118, 119). More recently, researchers found, for a couple of Fe-Al-Mo/W-Ti-B alloys with high boron contents to precipitate borides at grain boundaries, that these alloys maintained ductility at comparably low temperatures (Figure 7) (99, 120). This behavior is quite remarkable because in other intermetallic alloys the beneficial effect of adding boron disappears when borides form along grain boundaries (121). Moreover, an Fe-Al-Nb alloy doped with boron to precipitate a continuous film of Laves phase along the grain boundaries was ductile at comparably low temperatures [Fe-Al-Nb(B) in Figure 7] (104). The latter finding matches recent reports on steels strengthened by close-packed phases precipitated along grain boundaries (122). Apparently, although these phases are inherently brittle, no cracking occurs along or through these brittle phases as long as they form a more or less continuous grain boundary film on the order of  $1\text{-}\mu\text{m}$  thickness. In the case of the Laves phase,

compressive stresses at the grain boundaries may be one explanation for this astonishing observation. In the case of iron aluminides, films of borides or the Laves phase could also prevent ingress of moisture along grain boundaries, thereby inhibiting environmental embrittlement. In addition, precipitates at grain boundaries inhibit coarsening/abnormal grain growth at high temperatures (28, 89, 99).

Another possibility is that ductility may improve below some critical grain size (42). A compilation of various data from the literature indicates that, below a grain size of approximately 10  $\mu\text{m}$ , a substantial increase in ductility might be expected (123). Increased ductility has also been observed for fine-grained ( $<10\text{-}\mu\text{m}$ )  $\text{D0}_3$   $\text{Fe}_3\text{Al}$  obtained by refining with  $\text{TiB}_2$  (28), while  $\text{TiB}_2$ -refined B2 FeAl alloys with grain sizes of 40–50  $\mu\text{m}$  showed no improved ductility (124). However, this finding apparently cannot be generalized. Fe–30Al–10Ti with an average grain size of  $<5\ \mu\text{m}$  showed the same BDTT as its as-cast counterpart with an average grain size of  $>100\ \mu\text{m}$  (125). In contrast, an extremely coarse-grained and textured Fe–28Al alloy produced by additive manufacturing was ductile at room temperature (126). Whether the improved ductility of this alloy is due to internal stresses is not clear, as local X-ray diffraction investigations yielded no clear evidence. It has been frequently demonstrated that deformation processing can also improve ductility (14, 34, 127–130), although it is not clear whether, e.g., grain refinement or an increased number of mobile dislocations is responsible (123). **Figure 7** includes examples of the improvement in ductility after rolling, forging, or additive manufacturing.

As discussed above, vacancies have a strong hardening effect. As is the case for many other hardening mechanisms, ductility decreases simultaneously, probably because vacancies act as a solute for pinning dislocations (123). Consequently, ductility can improve by reducing the vacancy concentration through slow cooling and/or annealing at low temperature, although usually at the expense of strength (131–134).

#### 4.5. Fatigue

Data on fatigue of iron aluminides are comparably scarce (42). Only a few investigations have been performed on various alloy compositions by employing different test conditions. This scarcity of data prevents identification of general trends.

Most of the available information stems from the work of two groups, both of which focused on fatigue crack growth. Stoloff and coworkers studied  $\text{Fe}_3\text{Al}$ -based alloys (135, 137, 140), while the group of Henaff focused on FeAl alloys (136, 138). In agreement with other researchers (139), both groups found that environmental embrittlement by moist air has a major effect on fatigue crack growth in iron aluminides. Whether the mechanism for this environmental effect is embrittlement of the crack tip (111, 141) or lowering of the surface energy by adsorption of water vapor (142, 143) has not been conclusively settled. There seems to be no straightforward relation between ductility observed under static loading and ductility observed under cyclic loading (135). For example, Cr can improve the tensile ductility, but does not improve the fatigue behavior, of iron aluminides (141, 144, 145). The reason may be that Cr promotes the formation of an oxide film, which suppresses environmental embrittlement, but the oxide film may be repeatedly disrupted during fatigue cycling so that it is no longer protective (141, 146). In contrast, a small amount of Zr, which also promotes oxide film formation, showed a positive effect on ductility during both tensile and fatigue testing (147). Furthermore, alloying additions may have varying effects on fatigue crack growth rates when the number of cycles and/or loads is varied (135).

Investigation of high-cycle fatigue of binary Fe–24Al and Fe–29Al showed that the fatigue resistance improved when, instead of the single  $\text{D0}_3$  structure, a coherent two-phase  $\text{A2} + \text{D0}_3$

microstructure was present (148, 149). Moreover, anomalous strengthening in the temperature range of the YSA does not necessarily result in an increased fatigue life (150).

Analyses of the fractured surfaces revealed fracture by transgranular cleavage in most cases (144, 149, 151–153). However, the fracture mode may change from transgranular to a mixed mode and subsequently to intergranular if the environment becomes more aggressive in terms of environmental embrittlement (140, 154). By approximately 500°C, there are signs of ductile fracture (150), and the failure mode is a combination of fatigue cracking and cyclic creep (149, 152).

#### 4.6. Wear and Erosion

There are several investigations of the wear and erosion behavior of iron aluminides. However, due to some contradictory results and the variety of test methods, test conditions, and tested materials, it is difficult to draw general conclusions.

Iron aluminides possess good to excellent wear resistance that may equal or even outperform that of Cr steels (155, 156). A number of investigations evaluated the wear behavior, testing iron aluminides under various conditions as bulk alloys (157), coatings (158–162), binders for cemented hard phases (163, 164), and hard phases in ductile binders (165, 166). The wear resistance increases with increasing Al content, i.e., with increasing hardness (167, 168). The formation of an Al<sub>2</sub>O<sub>3</sub> oxide scale (169, 170), alloying additions to binary Fe–Al (155, 171), or addition of a hard second phase (168, 172, 173) can also improve the wear resistance. In contrast, the degree of long-range ordering in D0<sub>3</sub> Fe<sub>3</sub>Al has only a minor effect on wear (157), although a decrease in wear and erosion rates has been correlated with an increase in the critical temperature for the D0<sub>3</sub> ↔ B2 transition (155). The improvement in the wear resistance by an oxide scale has been attributed to an improvement in tribological properties by reducing the coefficient of friction (169). There is also an indication that environmental embrittlement may decrease the wear resistance, as a much higher weight loss has been observed after wet abrasion than after dry abrasion at otherwise identical conditions (174).

Iron aluminide bulk alloys and cermets show a ductile erosion behavior (160, 168, 175). Again, erosion resistance increases with increasing Al content. This behavior was attributed to an increase in strain hardening rates, which leads to rapid work hardening of the surface, thereby limiting deformation to a shallow region (175). For cermets, erosion resistance strongly depends on the microstructure rather than on hardness (168). Specifically, at high temperatures, at which oxidation plays a strong role, the erosion behavior of an iron aluminide outperforms that of a steel (156).

### 5. CORROSION

The outstanding property of the iron aluminide-based alloys is their corrosion resistance. They form dense and adherent Al<sub>2</sub>O<sub>3</sub> scales, which then protect the alloy against further attack by a hostile environment. The scales may form during service in oxidizing environments or can be generated by preoxidation.

#### 5.1. Oxidation

When research on the oxidation behavior of Fe–Al alloys started, one immediate finding was that, when approximately 8-wt% (15-at%) Al is added, an oxidation resistance is obtained that equals or surpasses that of heat-resistant steels (**Figure 8**) (176–178). Researchers later established that the minimum Al content necessary for Al<sub>2</sub>O<sub>3</sub> formation decreases with increasing temperature, i.e., from approximately 20-at% Al at 600°C to 10-at% Al at 1,000°C (**Figure 8**) (179, 180). This is the Al content necessary for the formation of dense and adherent  $\alpha$ -Al<sub>2</sub>O<sub>3</sub> scales, while at lower

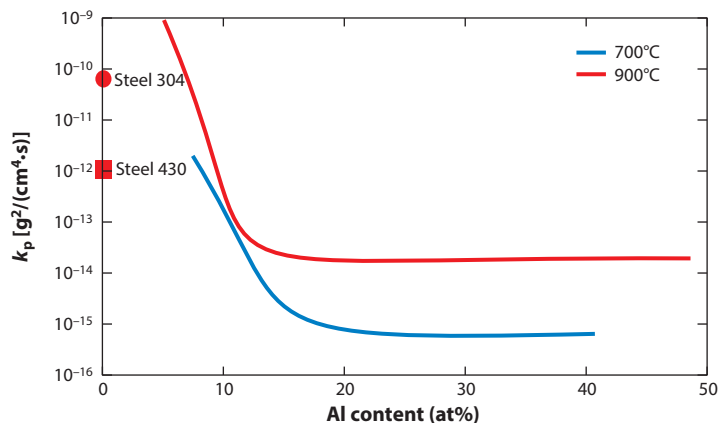


**Figure 8**

Parabolic rate constants  $k_p$  of binary Fe–Al at 700°C and 900°C in air as a function of Al content. Data for two Cr steels at 900°C are given for comparison and are from Reference 180.

Al contents, iron oxide scales or mixed oxide scales form. The formation of  $\alpha$ -Al<sub>2</sub>O<sub>3</sub> is preceded by the formation of metastable polymorphs like  $\Theta$ - and  $\gamma$ -Al<sub>2</sub>O<sub>3</sub>, which are porous and therefore less protective (181). Depending on variables such as temperature, alloy composition, and the partial pressures of oxygen and water vapor, a metastable hydroxide will initially form, and the type of hydroxide will determine the sequence of transformation to Al<sub>2</sub>O<sub>3</sub> (182, 183). The metastable phases are later undergrown by  $\alpha$ -Al<sub>2</sub>O<sub>3</sub> and finally also transform to  $\alpha$ -Al<sub>2</sub>O<sub>3</sub>, but this is a slow process (184). At 900°C, this transient period lasts approximately 100–150 h and becomes considerably shorter or longer at higher or lower temperatures, respectively (185–187).

Alloying has a marked effect on the oxidation behavior of Fe–Al. Most alloying additions impair the oxidation resistance, although not always in a detrimental way (181). The addition of Cr lowers the minimum Al content required for the formation of Al<sub>2</sub>O<sub>3</sub> scales (179). However, for Fe–28Al with up to 6-at% Cr, the scales grow faster and are therefore less adherent (188). Ni (179), Mo (189), Co (181), Mn (181), and many other elements neither improve nor deteriorate the oxidation resistance, while small additions of Y, Zr, or Hf improve scale adhesion (190–193). Temperature, oxygen partial pressure, and the concentration of the alloying addition have a crucial effect on the oxidation behavior. For all alloying additions, concentration limits exist beyond which the oxidation behavior deteriorates.

The little information that is available about the oxidation behavior in humid air or steam indicates that—even though the behavior can be quite different from that in dry air—binary or Hf-doped Fe–Al alloys form protective Al<sub>2</sub>O<sub>3</sub> scales at Al contents of approximately 20-at% Al or higher in these environments (194, 195). Fe–28Al–5Cr alloys with minor additions of Zr, Mo, and Nb even showed lower parabolic rate constants when tested in humid air relative to dry air, and this outcome was related to the faster transformation kinetics of the transient Al<sub>2</sub>O<sub>3</sub> polymorphs transforming to  $\alpha$ -Al<sub>2</sub>O<sub>3</sub> (196). Additionally, at elevated temperatures of 650–800°C, iron aluminide coatings showed excellent oxidation resistance in humid air or steam (197–199).

## 5.2. Sulfidation and Carburization

Iron aluminide-based alloys are also well known for their excellent sulfidation resistance (32, 87, 200). The basis for the good sulfidation resistance of binary iron aluminides is, again, the formation

of  $\text{Al}_2\text{O}_3$  scales (201). Alloying can have a varying effect on the sulfidation behavior, because, depending on the alloying addition, various scales may form, and again temperature and sulfur partial pressure play a crucial role (189, 202, 203). Preoxidation to form an  $\text{Al}_2\text{O}_3$  scale before exposure to a sulfidizing environment can markedly improve the corrosion resistance (204–206).

Few investigations have dealt with the carburizing behavior of iron aluminide alloys. At high temperatures (850–1,100°C), a couple of Fe–Al–Cr alloys showed no signs of carburization, presumably because a protective  $\text{Al}_2\text{O}_3$  scale had formed (203). At lower temperatures, resistance against metal dusting—i.e., disintegration into a fine mixture termed coke, which consists of graphite and fine metal particles or carbides—has been investigated (207–210). Systematic work on binary Fe–Al alloys revealed that resistance against metal dusting improved with increasing Al content and increasing temperature and that such resistance was again related to the formation of a protective  $\text{Al}_2\text{O}_3$  scale (208, 210). Investigators have also shown that metal dusting of Fe–Al can be reduced or even prohibited by further alloying (209), but comprehensive results are still missing.

### 5.3. Wet Corrosion

It has been claimed that the aqueous corrosion resistance of iron aluminides is poor (211, 212). This statement is true for many acidic, specifically  $\text{Cl}^-$ -containing, electrolytes. However, alloying can markedly improve wet corrosion resistance in specific electrolytes, and formation of a continuous oxide scale can substantially improve wet corrosion behavior even in strong acids. The aqueous corrosion resistance of Fe–Al has been examined mainly through electrochemical studies (reviewed in 213). According to these studies, the passivation behavior of Fe–Al is due to the combined effect of Al, which passivates through formation of an  $\text{Al}_2\text{O}_3$  film, and Fe, which passivates through the formation of iron oxide. During aqueous corrosion, protective films consisting of hydroxides or oxides of Al and Fe form. Relative to pure Fe, these films reduce the active dissolution of Fe–Al alloys, and the passivation and repassivation behavior of Fe–Al improves with increasing Al content (213, 214). The aqueous corrosion behavior of Fe–Al alloys varies in that they show passivation in neutral and alkaline environments but moderate to high corrosion rates in strong acids, specifically in the presence of  $\text{Cl}^-$ . Not much information is available about the effect of alloying elements on the aqueous corrosion behavior of Fe–Al. Cr generally improves the corrosion behavior of Fe–Al, specifically in combination with Mo (215, 216). There are conflicting reports as to whether aqueous corrosion resistance can be improved by formation of an  $\text{Al}_2\text{O}_3$  scale through preoxidation. For binary Fe–Al, a marked improvement was observed after preoxidation (217), while for alloyed Fe–Al, aqueous corrosion behavior sometimes deteriorated (218). That preoxidation is not in general effective in improving aqueous corrosion resistance has also been attributed to the fact that in some cases noncontinuous oxide scales formed on alloyed Fe–Al (219, 220). A general comparison of the aqueous corrosion behavior of Fe–Al with that of stainless steels is difficult, as results strongly depend on the electrolyte type. However, in many investigations of the aqueous corrosion resistance of iron aluminides, stainless steels were incorporated as a reference, and the corrosion resistance of the investigated Fe–Al alloys was often found to be comparable to that of the steels.

Few data are available on immersion tests. While weight losses after immersion in sulfuric acid continuously increased from pure Fe to Fe–Al containing 30-at% Al (221), immersion tests in seawater showed that corrosion resistance improved with increasing Al content (27). Neutral salt spray tests on binary Fe–Al revealed that corrosion resistance constantly improved up to an Al content of approximately 30 at% and that it could be further improved by addition of passivity-inducing elements (222). In the latter case, the improvement was related to the formation of dense

layers of  $\text{Fe}_3\text{O}_4$  (magnetite) during the tests (221, 222). For Fe–Al–Mo alloys, the resistance to salt spray surpasses that of stainless steel 403 (16).

#### 5.4. Hot Corrosion

Hot corrosion of iron aluminides, i.e., corrosion by salt deposits or salt melts at high temperatures, has been investigated to some extent (36, 223). Again, if the main corrosive attack during hot corrosion is by oxidation and if the Al content is sufficient for the formation of protective oxide scales, then iron aluminides show excellent corrosion resistance (224–226). If the main corrosive attack is not by oxidation, the corrosion resistance of iron aluminides can vary (36).

### 6. SYNTHESIS

Fe–Al alloys are usually produced from the pure elements by IM (induction melting). On a laboratory scale, VIM (vacuum induction melting) under inert gas is commonly employed, while in industry, melts from up to several thousand kilograms have been produced by AIM (air induction melting) and ESR (electroslag remelting) (25, 227). Exo-Melt<sup>TM</sup> is a melting procedure specifically developed for industrial production of nickel and iron aluminides (228). Melting in air is possible because the Fe–Al melts form a gas-tight slag, which prevents the underlying melt from further oxidation. Melting by other techniques, such as arc melting and electron beam melting, is also frequently used for the production of small amounts of alloys. Directional solidification and single-crystal growth have been performed using classical techniques like the Bridgman and floating zone techniques (229, 230). As for the case of Pyroferal, melting Fe–Al alloys from abundantly available scrap has been repeatedly investigated (231–233). Although production of homogeneous alloys by melting has been considered difficult (42), by all the abovementioned techniques, homogeneous alloys can be obtained.

Synthesis of Fe–Al alloys by various powder metallurgical methods has also been widely investigated. Consolidation by self-propagating high-temperature synthesis (234–237) or spark plasma sintering (238, 239) has been established to produce iron aluminides from mechanically alloyed elemental powders. The exothermic reaction between Fe and Al essentially helps in the consolidation of the powders, and iron aluminide +  $\text{Al}_2\text{O}_3$  composites have been produced via the thermite reaction (240).

### 7. PROCESSING

Processing of iron aluminide-based alloys by standard and nonstandard techniques is well established. Although processing parameters for specific alloys may vary, iron aluminides can be produced within the process windows used for Cr steels. Thermomechanical treatment in the disordered A2 condition as well as in the ordered B2 condition has been demonstrated (reviewed in 25, 32, 116, 241, 242).

#### 7.1. Casting

Ingots for further processing can be obtained by casting into steel molds, cast-iron molds, or Cu molds (at the laboratory scale). To avoid hydrogen-induced porosity/cracking, molds should be carefully dried. Cast parts have been successfully produced by various casting techniques, including sand casting, centrifugal casting, and precision casting (212, 228, 243). Strip casting has been employed for subsequent cold rolling of iron aluminides (244). Cast parts usually show good form

filling, low porosity, and smooth surfaces. However, if no measures are taken, Fe–Al casts can be rather coarse grained and can therefore easily crack. Casting of various parts on an industrial scale has been demonstrated (11, 12, 223, 228).

## 7.2. Forging

Cast ingots or consolidated powder samples are also frequently used as preforms for forging (29, 245–248). Although conditions for forging may vary depending on the specific alloys, the process windows are usually close to those used for Cr steels. Forging is specifically employed—as a first process step—for refining the microstructures of Fe–Al alloys, either (*a*) to break down the microstructure to obtain fine-grained alloys with enhanced ductility (249, 250) or (*b*) to redistribute precipitates (248). Duct halves and steam turbine and compressor blades have been produced by industrial forging (16, 23, 251, 252).

## 7.3. Rolling

The possibility of producing plates, sheets, and tapes by hot and cold rolling of iron aluminides has been frequently demonstrated (14, 253–255). Alloys with an Al content of up to approximately 30-at% Al may be processed according to the parameters used for rolling of Cr steels (129, 256). At higher Al contents, the rolling resistance becomes too high so that spacers have to be used or the alloys have to be canned (257, 258). Rolled products often show enhanced ductility, which has been explained by (*a*) the creation of mobile dislocations after short annealing; (*b*) reduced crack propagation by the formation of pancake-shaped grains; and (*c*) a reduction of environmental embrittlement (127, 259). However, ductility may be limited for coiling of sheets (260). From the produced sheets, laminated cores for magnetic applications and heating elements have been punched out (14, 254).

## 7.4. Powder Metallurgical Processing

As for most other intermetallic materials, powder metallurgical processing of iron aluminides has been investigated to some extent (261). Hot extrusion has been frequently performed to consolidate prealloyed powders, often with additions of oxides or borides to obtain dispersion-strengthened materials (28, 29, 262). Iron aluminide/steel tubes have been produced by coextruding the two materials (263), and ODS tubes have been investigated as well (264).

The production of samples and parts by additive manufacturing has been investigated using all currently employed techniques, e.g., selective laser melting (SLM), laser-engineered net shaping (LENS), laser metal deposition (LMD), and electron beam melting (EBM) (126, 265, 266). These techniques also allow for the production of chemically graded samples and parts (267).

## 7.5. Coatings

The outstanding feature of iron aluminides is their corrosion resistance. Therefore, much effort has been put toward the development of Fe–Al-based coatings (recently reviewed in 268, 269). Numerous compositions have been tested and used for the coating of various materials, but with some emphasis on coating of steels. High-velocity oxygen fuel spraying is the most widely used technique for the application of Fe–Al coatings, but other coating methods have also been extensively explored (270). The majority of the coatings have been developed for corrosion protection, although wear-resistant coatings are also of great interest (158–162). Fabrication on an industrial

scale has been demonstrated, and tests have been performed for applications in various environments (197, 198, 268, 271).

### 7.6. Machining

Machining of iron aluminides by all standard techniques such as grinding, turning, threading, and drilling has been demonstrated (272–274). However, “iron-aluminum alloys tend to work harden” and thus “sharp tools and slow speeds are required” (25, appendix A, p. 2). This wisdom from some 60 years ago is still essentially true. Experience from machining various parts showed that parameters can be not much different from those for machining high-Cr steels. However, parameters may vary for different Fe–Al alloys, and shortened tool lifetime and slow speeds have to be taken into account. Therefore, economical cutting of iron aluminides on an industrial scale is a critical issue (275).

### 7.7. Welding

Welding of iron aluminides is possible, but “the weldability of these alloys is very sensitive to the welding conditions, producing good welds sometimes and severely cracked welds at other times” (276, p. s372). Pre- and postweld heat treatments can help to avoid cracking by lowering thermal stresses and driving off residual hydrogen (277, 278). Joints of iron aluminides or of iron aluminide and steels have been made, the latter preferentially by diffusion bonding. Although different techniques have been successfully tested, friction stir welding was employed for the more demanding welding of boride-containing and ODS Fe–Al alloys (279–281).

## 8. APPLICATIONS

Despite the appealing properties of iron aluminides (i.e., excellent corrosion and wear resistance and comparably low density) and their economic attractiveness, few applications have been realized. Although many of the obvious applications have been explored on an industrial scale, few of these undertakings are documented. Use of Pyroferal stopped when strategic elements for the production of stainless steels became available again after the end of World War II. Pyroferal was mainly used in industrial furnace equipment, e.g., for pyrite roasting or carburizing; in the aluminum industry; and for cast turbine parts (11, 12). All these applications have been revisited (24, 212, 228, 252). Turbocharger parts (282) and exhaust valves have been widely explored and produced for automotive applications (34). Brake discs could be another interesting application, although a single piece of published evidence is not in favor of this application (283). Tubes and pipes—consisting of iron aluminide; coated by iron aluminides; consisting of a dual iron aluminide/steel compound structure; or with continuous steel/iron aluminide compositional gradients produced, e.g., by pack cementation—have been produced for applications in numerous environments (227, 264, 271, 284, 285). Additionally, use of iron aluminide as cutting blade materials for cutlery or industrial cutting applications has been investigated to some extent (16, 286). NASA has also identified iron aluminides as a possible lunar engineering material, as it accrues as a by-product of the production of oxygen and silicon on the moon (287).

Among functional applications, sintered iron aluminide filter elements for hot-gas cleaning are commercially available (288, 289), and high-temperature filtering of fumes for separation of arsenic and antimony oxides is currently being investigated (290). More recently, the different iron aluminide phases have been explored as catalysts.  $\text{D}_0_3 \text{Fe}_3\text{Al}$  doped with ruthenium has been

considered for the electrosynthesis of sodium chlorate and  $\text{Al}_{13}\text{Fe}_4$  as an active and selective semi-hydrogenation catalyst (291, 292).

Lack of strength at high temperatures and limited ductility at ambient temperature, both of which have not been solved by classical alloying concepts like strengthening by carbides, have so far precluded the wider use of iron aluminide-based alloys. New alloy concepts paired with the need for cheaper, more sustainable, and more heat-resistant materials have evoked considerable interest by industries again. A number of efforts are under way to (re)evaluate the use of iron aluminide-based alloys for aeronautical, automotive, naval, and energy conversion applications.

## DISCLOSURE STATEMENT

The authors are not aware of any affiliations, memberships, funding, or financial holdings that might be perceived as affecting the objectivity of this review.

## LITERATURE CITED

1. Keep WJ. 1890. Aluminum in cast iron. *Trans. AIME* 18:102–22
2. Hadfield RA. 1890. Aluminium-steel. *J. Iron Steel Inst.* 2:161–230
3. Guillet L. 1902. Les alliages d'aluminium [The alloys of aluminum]. *Génie Civ.* 41:377–82
4. Durnenko HF. 1934. Aluminevy cugun (Cugal) [Aluminum containing cast iron]. *Liteisick* No. 7
5. Smirnov VI, Neroveckaia GI. 1940. Issledovanie svojstvo zaroupornvch aluminiyevych cuganov [Investigation of the properties of aluminum containing cast iron]. *Metallurg* 3:12–21
6. BCIRA, Bampfyld JW. 1938. *Improvements in and relating to the manufacture of cast iron alloys*. UK Patent GB489936
7. Milman BS, Klotchnev NI, Aleksandrov NN, Kovalevich EV, Popova NY. 1961. *Zharostojkij chugun [Heat-resistant cast iron]*. Sov. Union Patent SU135500
8. Pluhar J, Vyklicky M. 1954. Úsporné záruvzdorné slitiny pro teploty nad 800°C [Applicable heat-resistant alloys for temperatures above 800°C]. *Slevarenstvi* 4:9–16 (In Czech)
9. Pluhar J, Vyklicky M. 1956. *Svařitelná záruvzdorná litina s obsahem bliníku [Weldable heat-resistant aluminum containing cast iron]*. Czech Patent SPIS c. 84598:1–2 (In Czech)
10. Pluhar J, Vyklicky M. 1959. *Vlastnosti záruvzdorné slitiny čsn 42 2482 (Pyroferal) a její použití [Properties of the heat-resistant alloy CSN 42 2484 (Pyroferal) and its use]*. Tech. Rep. 189, Ministry of the Heavy Industry, Prague (In Czech)
11. Kratochvil P. 2008. The history of the search and use of heat resistant Pyroferal alloys based on FeAl. *Intermetallics* 16:587–91
12. Eminger Z. 1957. Beitrag zur Frage der Herstellung von Gußstücken aus der Eisen-Aluminium-Legierung “Pyroferal” [Contribution to the question on the production of cast pieces of the iron-aluminum-alloy “Pyroferal”]. *Freib. Forsch. B* 24-I:121–44 (In German)
13. Nachman JF, Buehler WJ. 1953. *The fabrication and properties of 16-ALFENOL—a non-strategic aluminum-iron alloy*. US Nav. Ord. Lab. (NAVORD) Rep. 2819, Silver Spring, MD
14. Nachman JF, Buehler WJ. 1954. 16 percent aluminum-iron alloy cold rolled in the order-disorder temperature range. *J. Appl. Phys.* 25:307–13
15. Nachman JF, Buehler WJ. 1954. *Thermenol—a non-strategic aluminum-iron base alloy for high temperature service*. NAVORD Rep. 3700
16. Nachman JF, Buehler WJ. 1956. Fe-Al-Mo alloys for high-temperature use. *Met. Prog.* 70:107–10
17. Morgan ER, Zackay VF. 1955. Ductile iron aluminum alloys. *Met. Prog.* 68:126–28
18. Morgan ER. 1955. *Method of preparation of iron aluminum alloys*. US Patent US2726952A
19. Justusson W, Zackay VF, Morgan ER. 1957. The mechanical properties of iron-aluminum alloys. *Trans. ASM* 49:905–23
20. Tate F. 1959. *Development of iron-aluminum base alloy for gas cooled reactor components*. Final Rep. MND-DB-2525, Off. Tech. Serv., US Dep. Commer.

21. Mueller JJ, Tate FG. 1961. *Iron-aluminum base alloys*. US Patent US2987394 A
22. Chubb W, Alfant S, Bauer AA, Jablonowski EJ, Shober FR, Dickerson RF. 1958. *Constitution, metallurgy, and oxidation resistance of iron-chromium-aluminum alloys*. Rep. BMI-1298, Batelle Meml. Inst.
23. Buehler WJ, Dalrymple CG. 1958. Coming: better Thermenol alloys. *Met. Prog.* 73:78-81
24. Brooks R, Volio A. 1959. *Iron-aluminum alloy systems. Part 14: Welding of iron-aluminum alloys*. Wright Air Dev. Cent. (WADC) Tech. Rep. 57-298, WADC, Wright Patterson Airforce Base, OH
25. Lepkowski WJ, Holladay JW. 1957. *The present state of development of iron-aluminum-base alloys*. Rep. NP-6509, Batelle Meml. Inst.
26. Holladay JW. 1961. *Review of developments in iron-aluminum-base alloys*. Rep. NTIS (OTS) PB 161232, Batelle Meml. Inst.
27. Nachman JF, Duffy ER. 1974. Effect of alloying additions on sea water corrosion resistance of iron-aluminum base alloys. *Corrosion* 30:357-65
28. Bordeau RG. 1987. *Development of iron aluminides*. Rep. AFWAL-TR-87-4009, Air Force Wright Aeronaut. Lab.
29. Culbertson G, Kortovich CS. 1986. *Development of iron aluminides*. Rep. AFWAL-TR-85-4155, Air Force Wright Aeronaut. Lab.
30. Oak Ridge Natl. Lab. 1987-2001. *Proceedings of the annual conference on fossil energy materials*. Conf. Ser., Oak Ridge Natl. Lab., Oak Ridge, TN
31. Liu CT, Lee EH, McKamey CG. 1989. An environmental effect as the major cause for room-temperature embrittlement in FeAl. *Scr. Metall.* 23:875-80
32. McKamey CG. 1996. Iron aluminides. See Ref 302, pp. 351-91
33. McKamey CG, DeVan JH, Tortorelli PF, Sikka VK. 1991. A review of recent developments in Fe<sub>3</sub>Al-based alloys. *J. Mater. Res.* 6:1779-805
34. Deevi SC, Sikka VK. 1996. Nickel and iron aluminides: an overview on properties, processing, and applications. *Intermetallics* 4:357-75
35. Liu CT, George EP, Maziasz PJ, Schneibel JH. 1998. Recent advances in B2 iron aluminide alloys: deformation, fracture and alloy design. *Mater. Sci. Eng. A* 258:84-98
36. Tortorelli PF, Natesan K. 1998. Critical factors affecting the high-temperature corrosion performance of iron aluminides. *Mater. Sci. Eng. A* 258:115-25
37. Moret F, Baccino R, Martel P, Guetaz L. 1996. Propriétés et applications des alliages intermétalliques B2-FeAl [Properties and applications of intermetallic B2-FeAl alloys]. *J. Phys. IV Fr.* 6:C2-281-89
38. Revol S, Baccino R, Moret F. 2000. Industrial applications of FeAl40Grade3, a high specific properties iron aluminides. In *Intermetallics and Superalloys*, Vol. 10, ed. DG Morris, S Naka, P Caron, pp. 307-11. Weinheim, Ger.: Wiley-VCH
39. Morris DG, Morris MA. 1997. Strengthening at intermediate temperatures in iron aluminides. *Mater. Sci. Eng. A* 239:23-38
40. Morris DG, Muñoz-Morris MA. 2010. A re-examination of the pinning mechanisms responsible for the stress anomaly in FeAl intermetallics. *Intermetallics* 18:1279-84
41. Sauthoff G. 1995. *Intermetallics*. Weinheim, Ger.: Wiley-VCH
42. Vedula K. 1995. FeAl and Fe<sub>3</sub>Al. See Ref 300, pp. 199-209
43. Stein F, Palm M. 2007. Re-determination of transition temperatures in the Fe-Al system by differential thermal analysis. *Int. J. Mater. Res.* 98:580-88
44. Schneibel JH. 1994. Selected properties of iron aluminides. See Ref 303, pp. 329-42
45. Taylor A, Jones RM. 1958. Constitution and magnetic properties of iron-rich iron-aluminum alloys. *J. Phys. Chem. Solids* 6:16-37
46. Köster W, Gödecke T. 1981. Physikalische Messungen an Eisen-Aluminium-Legierungen mit 10 bis 50 At.-% Al. II. Die Ausdehnungskoeffizienten der Legierungen mit 10 bis 35 At.-% Al [Physical measurements of iron-aluminum alloys with 10 to 50 at.-% Al. II. (Thermal) expansion coefficients of alloys with 10 to 35 at.-% Al]. *Z. Metallkd.* 72:569-74
47. Köster W, Gödecke T. 1981. Physikalische Messungen an Eisen-Aluminium-Legierungen mit 10 bis 50 At.-% Al. III. Die Ausdehnungskoeffizienten der Legierungen mit 20 bis 50 At.-% Al

- [Physical measurements of iron-aluminum alloys with 10 to 50 at.-% Al. III. (Thermal) expansion coefficients of alloys with 20 to 50 at.-% Al]. *Z. Metallkd.* 72:707–11
48. Ruan Y, Yan N, Zhu HZ, Zhou K, Wei B. 2017. Thermal performance determination of binary Fe-Al alloys at elevated temperatures. *J. Alloys Compd.* 701:676–81
  49. Köster W, Gödecke T. 1982. Physikalische Messungen an Eisen-Aluminium-Legierungen mit 10 bis 50 At.-% Al. IV. Der Elastizitätsmodul der Legierungen [Physical measurements of iron-aluminum alloys with 10 to 50 at.-% Al. IV. Young's modulus of the alloys]. *Z. Metallkd.* 73:111–14
  50. Mehrer H, Eggersmann M, Gude A, Salamon M, Sepiol B. 1997. Diffusion in intermetallic phases of the Fe-Al and Fe-Si systems. *Mater. Sci. Eng. A* 239–240:889–98
  51. Eggersmann M, Mehrer H. 2000. Diffusion in intermetallic phases of the Fe-Al system. *Philos. Mag. A* 80:1219–44
  52. Rudajevová A, Buriánek J. 2001. Determination of thermal diffusivity and thermal conductivity of Fe-Al alloys in the concentration range 22 to 50 at.-% Al. *J. Phase Equilib.* 22:560–63
  53. Lilly AC, Deevi SC, Gibbs ZP. 1998. Electrical properties of iron aluminides. *Mater. Sci. Eng. A* 258:42–49
  54. Reddy BV, Jena C, Deevi SC. 2000. Electronic structure and transport properties of Fe–Al alloys. *Intermetallics* 8:1197–207
  55. Okamoto H, Beck PA. 1971. Phase relationships in the iron-rich Fe-Al alloys. *Metall. Trans.* 2:569–74
  56. Hernando A, Amils X, Nogués J, Surinach S, Baró MD, Ibarra MR. 1998. Influence of magnetization on the reordering of nanostructured ball-milled Fe-40 at.-% Al powders. *Phys. Rev. B* 58:R11864–67
  57. Yang Y, Baker I, Martin P. 1999. On the mechanism of the paramagnetic-to-ferromagnetic transition in Fe-Al. *Philos. Mag. B* 79:449–61
  58. Menéndez E, Liedke MO, Fassbender J, Gemming T, Weber A, et al. 2009. Direct magnetic patterning due to the generation of ferromagnetism by selective ion irradiation of paramagnetic FeAl alloys. *Small* 5:229–34
  59. Varea A, Menéndez E, Montserrat J, Lora-Tamayo E, Weber A, et al. 2011. Tuneable magnetic patterning of paramagnetic Fe<sub>60</sub>Al<sub>40</sub> (at. %) by consecutive ion irradiation through pre-lithographed shadow masks. *J. Appl. Phys.* 109:093918
  60. Polushkin NI, Oliveira V, Vilar R, He M, Shugaev MV, Zhigilei LV. 2018. Phase-change magnetic memory: rewritable ferromagnetism by laser quenching of chemical disorder in Fe<sub>60</sub>Al<sub>40</sub> alloy. *Phys. Rev. Appl.* 10:024023
  61. Schaefer H-E, Würschum R, Sob M, Zak T, Yu WZ, et al. 1990. Thermal vacancies and positron-lifetime measurements in Fe<sub>76.3</sub>Al<sub>23.7</sub>. *Phys. Rev. B* 41:11869–74
  62. Wolff J, Franz M, Hehenkamp T. 1997. Defect analysis with positron annihilation—applications to Fe aluminides. *Mikrochim. Acta* 125:263–68
  63. Broska A, Wolff J, Franz M, Hehenkamp T. 1999. Defect analysis in FeAl and FeSi with positron lifetime spectroscopy and Doppler broadening. *Intermetallics* 7:259–67
  64. Rieu J, Goux C. 1969. Etude du durcissement par trempe des alliages ordonnés Fe-Al de type L2<sub>0</sub> [Investigation of the hardness after quenching of ordered Fe–Al alloys of type L2<sub>0</sub>]. *Mem. Sci. Rev. Metall.* 66:869–80
  65. Würschum R, Grupp C, Schaefer H-E. 1995. Simultaneous study of vacancy formation and migration at high temperatures in B2-type Fe aluminides. *Phys. Rev. Lett.* 75:97–100
  66. Hasemann G, Schneibel JH, George EP. 2012. Dependence of the yield stress of Fe<sub>3</sub>Al on heat treatment. *Intermetallics* 21:56–61
  67. Yang Y, Baker I. 1998. The influence of vacancy concentration on the mechanical behavior of Fe-40Al. *Intermetallics* 6:167–75
  68. Dlubek G, Brümmer O, Möser B. 1982. The recovery of quenched-in vacancies in Fe-Al (6.3 to 28.3 at.-%) alloys studied by positron annihilation. *Cryst. Res. Technol.* 17:951–61
  69. Cizek J, Lukac F, Melikhova O, Prochazka I, Kuzel R. 2011. Thermal vacancies in Fe<sub>3</sub>Al studied by positron annihilation. *Acta Mater.* 59:4068–78
  70. Stein F, Schneider A, Frommeyer G. 2003. Flow stress anomaly and order-disorder transitions in Fe<sub>3</sub>Al-based Fe-Al-Ti-X alloys with X = V, Cr, Nb, or Mo. *Intermetallics* 11:71–82

71. Davies RG, Stoloff NS. 1963. Work hardening in Fe<sub>3</sub>Al. *Acta Metall.* 11:1187–89
72. Morris DG, Muñoz-Morris MA. 2005. The stress anomaly in FeAl-Fe<sub>3</sub>Al alloys. *Intermetallics* 13:1269–74
73. Nishino Y, Ogawa K, Tanaka H. 2012. Internal friction study of vacancy hardening in B2 Fe Al alloys. *Solid State Phenom.* 184:81–86
74. Morris DG, Muñoz-Morris MA. 2014. High-temperature creep of iron aluminide intermetallics. In *Encyclopedia of Thermal Stresses*, ed. RB Hetnarski, pp. 2226–36. Dordrecht, Neth.: Springer
75. George EP, Baker I. 1998. Thermal vacancies and the yield strength anomaly of FeAl. *Intermetallics* 6:759–63
76. Baker I, Gaydos DJ. 1987. Flow and fracture of Fe-Al. *Mater. Sci. Eng.* 96:147–58
77. Guo JT, Jin O, Yin WM, Wang TM. 1993. Discovery and study of anomalous yield strength peak in FeAl alloy. *Scr. Metall. Mater.* 29:783–85
78. Yoshimi K, Hanada S, Yoo MH. 1995. Yielding and plastic flow behavior of B2-type Fe-39.5 mol.% single crystals in compression. *Acta Metall. Mater.* 43:4141–51
79. Umakoshi Y, Yamaguchi M. 1980. Deformation of FeAl single crystals at high temperatures. *Philos. Mag. A* 41:573–88
80. Yoshimi K, Yoo MH, Hanada S. 1998. Slip band propagation and slip vector transition in B2 FeAl single crystals. *Acta Mater.* 46:5769–76
81. Schaefer H-E, Frenner K, Würschum R. 1999. High-temperature atomic defect properties and diffusion processes in intermetallic compounds. *Intermetallics* 7:277–87
82. Morris DG, Zhao P, Muñoz-Morris MA. 2001. An examination of the influence of strain rate on the stress anomaly in Fe<sub>3</sub>Al. *Mater. Sci. Eng. A* 297:256–65
83. Schmatz DJ, Bush RH. 1968. Elevated temperature yield effect in iron-aluminum. *Acta Metall.* 16:207–17
84. Song JH, Ha TK, Chang YW. 2000. Anomalous temperature dependence of flow stress in a Fe<sub>3</sub>Al alloy. *Scr. Mater.* 42:271–76
85. Krein R, Palm M. 2007. Two-fold flow stress anomaly in L2<sub>1</sub>-ordered Fe-Al-Ti based alloys. *Mater. Sci. Eng. A* 460–461:174–79
86. Hardwick D, Wallwork G. 1978. Iron-aluminium alloys: a review of their feasibility as high-temperature materials. *Rev. High Temp. Mater.* 4:47–74
87. Mendiratta MG, Ehlers SK, Dimiduk DM, Kerr WR, Mazdiyasi S, Lipsitt HA. 1987. A review of recent developments in iron aluminides. *Mater. Res. Soc. Symp. Proc.* 81:393–404
88. Morris DG. 1998. Possibilities for high-temperature strengthening in iron aluminides. *Intermetallics* 6:753–58
89. Bahadur A. 2003. Enhancement of high temperature strength and room temperature ductility of iron aluminides by alloying. *Mater. Sci. Technol.* 19:1627–34
90. Palm M. 2005. Concepts derived from phase diagram studies for the strengthening of Fe-Al-based alloys. *Intermetallics* 13:1286–95
91. Kayser FX. 1958. Effect of order on the plastic behavior of iron-aluminum alloys. *J. Met.* 10:573
92. Morgand P, Mouturat P, Sainfort G. 1968. Structure et propriétés mécaniques des alliages fer-aluminium. *Acta Metall.* 16:867–75
93. Marcinkowski MJ. 1974. The relationship between atomic order and the mechanical properties of alloys. In *Treatise in Materials Science and Technology*, Vol. 5, ed. H Herman, pp. 181–287. New York: Academic
94. Lawley A, Coll JA, Cahn RW. 1960. Influence of crystallographic order on creep of iron-aluminum solid solutions. *Trans. AIME* 218:166–76
95. Cahn RW. 2002. How does long-range order affect creep of alloys? *Mater. Sci. Eng. A* 324:1–4
96. Sauthoff G. 1995. Plastic deformation. See Ref 299, pp. 911–34
97. Whittenberger JD. 1986. The influence of grain size and composition on slow plastic flow in FeAl between 1100 and 1400 K. *Mater. Sci. Eng.* 77:103–13
98. Doucakis T, Kumar KS. 1999. Formation and stability of refractory metal diborides in an Fe<sub>3</sub>Al matrix. *Intermetallics* 7:765–77

99. Krein R, Schneider A, Sauthoff G, Frommeyer G. 2007. Microstructure and mechanical properties of Fe<sub>3</sub>Al-based alloys with strengthening boride precipitates. *Intermetallics* 15:1172–82
100. Song G, Sun Z, Li L, Xu X, Rawlings M, et al. 2015. Ferritic alloys with extreme creep resistance via coherent hierarchical precipitates. *Sci. Rep.* 5:16327
101. Dimiduk DM, Mendiratta MG, Banerjee D, Lipsitt HA. 1988. A structural study of ordered precipitates in an ordered matrix within the Fe-Al-Nb system. *Acta Metall.* 36:2947–58
102. Risanti DD, Sauthoff G. 2011. Microstructures and mechanical properties of Fe-Al-Ta alloys with strengthening Laves phase. *Intermetallics* 19:1727–36
103. Prokopcakova P, Svec M, Palm M. 2016. Microstructural evolution and creep of Fe-Al-Ta alloys. *Int. J. Mater. Res.* 107:396–405
104. Azmi SA, Michalcová A, Sencekova L, Palm M. 2017. Microstructure and mechanical properties of Fe-Al-Nb-B alloys. *MRS Adv.* 2:1353–59
105. Tarigan I, Kurata K, Takata N, Matsuo T, Takeyama M. 2011. Novel concept for creep strengthening mechanism using grain boundary Fe<sub>2</sub>Nb Laves phase in austenitic heat resistant steel. *Mater. Res. Soc. Symp. Proc.* 1295:317–22
106. Niewolak L, Savenko A, Grüner D, Hattendorf H, Breuer U, Quadackers WJ. 2015. Temperature dependence of Laves phase composition in Nb, W and Si-alloyed high chromium ferritic steels for SOFC interconnect applications. *J. Phase Equil. Diffus.* 36:471–84
107. Nishino Y, Asano S, Ogawa T. 1997. Phase stability and mechanical properties of Fe<sub>3</sub>Al with addition of transition elements. *Mater. Sci. Eng. A* 234–36:271–74
108. Ohnuma I, Schön CG, Kainuma R, Inden G, Ishida K. 1998. Ordering and phase separation in the b.c.c. phase of the Fe-Al-Ti system. *Acta Mater.* 46:2083–94
109. Krein R, Friak M, Neugebauer J, Palm M, Heilmaier M. 2010. L2<sub>1</sub>-ordered Fe-Al-Ti alloys. *Intermetallics* 18:1360–64
110. Liu CT, McKamey CG, Lee EH. 1990. Environmental effects on room temperature ductility and fracture in Fe<sub>3</sub>Al. *Scr. Metall. Mater.* 24:385–90
111. Stoloff NS, Liu CT. 1994. Environmental embrittlement of iron aluminides. *Intermetallics* 2:75–84
112. Zamanzade M, Barnoush A, Motz C. 2016. A review on the properties of iron aluminide intermetallics. *Crystals* 6:10
113. Schulson EM. 1996. Brittle fracture and toughening. See Ref 302, pp. 56–94
114. Kimura Y, Pope DP. 1998. Ductility and toughness in intermetallics. *Intermetallics* 6:567–71
115. Risanti D, Deges J, Falat L, Kobayashi S, Konrad J, et al. 2005. Dependence of the brittle-to-ductile transition temperature (BDTT) on the Al content of Fe-Al alloys. *Intermetallics* 13:1337–42
116. Palm M. 2009. Fe-Al materials for structural applications at high temperatures: current research at MPIE. *Int. J. Mater. Res.* 100:277–87
117. Fraczkiewicz A, Gay A-S, Biscondi M. 1998. On the boron effect in FeAl (B2) intermetallic alloys. *Mater. Sci. Eng. A* 258:108–14
118. Liu CT, George EP. 1991. Effect of aluminum concentration and boron dopant on environmental embrittlement in FeAl aluminides. *Mater. Res. Soc. Symp. Proc.* 213:527–32
119. Fraczkiewicz A. 2000. Influence of boron on the mechanical properties of B2-ordered FeAl alloys. *Mater. Trans. JIM* 41:166–69
120. Li X, Prokopcakova P, Palm M. 2014. Microstructure and mechanical properties of Fe-Al-Ti-B alloys with additions of Mo and W. *Mater. Sci. Eng. A* 611:234–41
121. Briant CL. 1995. Intergranular and cleavage fracture. See Ref 299, pp. 895–910
122. Kanno N, Yoshimura K, Takata N, Tarigan I, Takeyama M. 2016. Mechanical properties of austenitic heat-resistant Fe-20Cr-30Ni-2Nb steel at ambient temperature. *Mater. Sci. Eng. A* 662:551–63
123. Morris DG, Morris-Muñoz MA. 1999. The influence of microstructure on the ductility of iron aluminides. *Intermetallics* 7:1121–29
124. McKamey CG, Liu CT, Cathcart JV, David SA, Lee EH. 1986. *Evaluation of mechanical and metallurgical properties of Fe<sub>3</sub>Al-based alloys*. Rep. ORNL/TM-10125, Oak Ridge Natl. Lab., Oak Ridge, TN
125. Michalcová A, Sencekova L, Rolink G, Weisheit A, Pesicka J, et al. 2016. Laser additive manufacturing of iron aluminides strengthened by ordering, borides or coherent Heusler phase. *Mater. Des.* 116:481–94

126. Rolink G, Vogt S, Sencekova L, Weisheit A, Poprawe R, Palm M. 2014. Laser metal deposition and selective laser melting of Fe–28 at. % Al. *J. Mater. Res.* 29:2036–43
127. McKamey CG, Pierce DH. 1993. Effect of recrystallization on room temperature tensile properties of an Fe<sub>3</sub>Al-based alloy. *Scr. Metall. Mater.* 28:1173–76
128. Sanders PG, Sikka VK, Howell CR, Baldwin RH. 1991. A processing method to reduce the environmental effect in Fe<sub>3</sub>Al-based alloys. *Scr. Metall. Mater.* 25:2365–69
129. Konrad J, Zaeferrer S, Schneider A, Raabe D, Frommeyer G. 2005. Hot deformation behavior of a Fe<sub>3</sub>Al-binary alloy in the A2 and B2-order regimes. *Intermetallics* 13:1304–12
130. Hanus P, Bartsch E, Palm M, Krein R, Bauer-Partenheimer K, Janschek P. 2010. Mechanical properties of a forged Fe–25Al–2Ta steam turbine blade. *Intermetallics* 18:1379–84
131. Gaydosch DJ, Nathal MV. 1990. Influence of testing environment on the room temperature ductility of FeAl alloys. *Scr. Metall. Mater.* 24:1281–84
132. Baker I, Nagpal P. 1993. A review of the flow and fracture of FeAl. In *Structural Intermetallics*, ed. R Darolia, JJ Lewandowski, CT Liu, PL Martin, DB Miracle, MV Nathal, pp. 463–73. Warrendale, PA: TMS
133. Yoshimi K, Hanada S, Tokuno H. 1994. Effect of frozen-in vacancies on hardness and tensile properties of polycrystalline B2 FeAl. *Mater. Trans. JIM* 35:51–57
134. Jordan JL, Deevi SC. 2003. Vacancy formation and effects in FeAl. *Intermetallics* 11:507–28
135. Stoloff NS, Alven DA, McKamey CG. 1997. An overview of Fe<sub>3</sub>Al alloy development with emphasis on creep and fatigue. In *International Symposium on Nickel and Iron Aluminides: Processing, Properties, and Applications*, ed. SC Deevi, PJ Maziasz, VK Sikka, RW Cahn, pp. 65–72. Materials Park, OH: ASM Int.
136. Henaff G, Benoit G, Comyn M, Jouiad M. 2010. Fatigue crack growth resistance of a Fe-40Al grade 3 alloy prepared by mechanical alloying and forging. *Proc. Eng.* 2:1431–40
137. Stoloff NS. 1997. Fatigue crack growth in intermetallics. In *Structural Intermetallics 1997*, ed. MV Nathal, R Darolia, CT Liu, PL Martin, DB Miracle, et al., pp. 33–42. Warrendale, PA: TMS
138. Tonneau A, Gerland M, Henaff G. 2001. Environment-sensitive fracture of iron aluminides during cyclic crack growth. *Metall. Mater. Trans. A* 32:2345–56
139. Hanes DB, Gibala R. 1997. Low cycle fatigue of FeAl (42 at. % Al) at room temperature. *Mater. Res. Soc. Symp. Proc.* 460:361–66
140. Stoloff NS, Castagna A, Scott J, Duquette DJ. 1994. Environmental embrittlement of Fe<sub>3</sub>Al alloys under monotonic and cyclic loading. See Ref 303, pp. 271–85
141. Castagna A, Stoloff NS. 1992. The influence of environment on fatigue crack growth of an Fe<sub>3</sub>Al, Cr alloy. *Scr. Metall. Mater.* 26:673–78
142. Tonneau A, Henaff G. 2001. Tensile and fatigue properties as influenced by environment of a FeAl alloy prepared by mechanical alloying. *J. Phys. IV Fr.* 11:321–28
143. Henaff G, Tonneau A. 2001. Environmental embrittlement of a FeAl alloy prepared by mechanical alloying under monotonic and cyclic loading. In *Structural Intermetallics 2001*, ed. KJ Hemker, DM Dimiduk, H Clemens, R Darolia, H Inui, et al., pp. 571–80. Warrendale, PA, USA: TMS
144. Schneibel JH, Rühle H, Heilmaier M, Saage H, Goncharenko M, Loboda P. 2010. Low cycle fatigue of Fe<sub>3</sub>Al-based iron aluminide with and without Cr. *Intermetallics* 18:1369–74
145. Gang F, Krüger M, Laskosky A, Rühle H, Schneibel JH, Heilmaier M. 2011. Fatigue resistance of Fe<sub>3</sub>Al-based alloys. *Mater. Res. Soc. Symp. Proc.* 1295:59–64
146. Tonneau A, Henaff G, Gerland M, Petit J. 1998. Fatigue crack propagation resistance of a FeAl-based alloy. *Mater. Sci. Eng. A* 256:256–64
147. Alven DA, Stoloff NS. 1996. Fatigue crack growth of Fe<sub>3</sub>Al,Cr alloys. *Scr. Mater.* 34:1937–42
148. Stoloff NS, Fuchs GE, Kuruvilla AK, Choe SJ. 1987. Fatigue of intermetallic compounds. *Mater. Res. Soc. Symp. Proc.* 81:247–61
149. Fuchs GE, Stoloff NS. 1988. Effects of temperature, ordering and composition on high cycle fatigue of polycrystalline Fe<sub>3</sub>Al. *Acta Metall.* 36:1381–87
150. Yasuda HY, Behgozin A, Umakoshi Y. 1999. Fatigue behavior of Fe–48at.% Al polycrystals with B2 structure at high temperatures. *Scr. Mater.* 40:203–7

151. Hausild P, Karlik M, Siegl J, Nedbal I. 2005. Fractographic analysis of the crack growth in the Fe<sub>3</sub>Al based intermetallic alloy. *Intermetallics* 13:217–25
152. Jaske CE, Deevi SC, Shademan SS. 1988. Fatigue and cyclic deformation behavior of iron aluminide. *Mater. Sci. Eng. A* 258:211–18
153. Karlik M, Nedbal I, Siegl J, Prah J. 2004. Behaviour of an Fe-28Al-3Cr-Ce alloy under cyclic loading. *J. Alloys Compd.* 378:263–67
154. Castagna A, Maziasz PJ, Stoloff NS. 1993. Influence of environment on crack growth resistance of an Fe<sub>3</sub>Al,Cr alloy. *Mater. Res. Soc. Symp. Proc.* 288:1043–48
155. Johnson M, Mikkola DE, March PA, Wright RN. 1990. The resistance of nickel and iron aluminides to cavitation erosion and abrasive wear. *Wear* 140:279–89
156. Magnee A. 1995. Generalized law of erosion: application to various alloys and intermetallics. *Wear* 181–183:500–10
157. Maupin HE, Wilson RD, Hawk JA. 1992. An abrasive wear study of ordered Fe<sub>3</sub>Al. *Wear* 159:241–47
158. Chen Y, Wang HM. 2003. Microstructure and wear resistance of laser clad TiC reinforced FeAl intermetallic matrix composite coatings. *Surf. Coat. Technol.* 168:30–36
159. Xu B, Zhu Z, Ma S, Zhang W, Liu W. 2004. Sliding wear behavior of Fe–Al and Fe–Al/WC coatings prepared by high velocity arc spraying. *Wear* 257:1089–95
160. Guilemany JM, Cinca N, Fernandez J, Sampath S. 2008. Erosion, abrasive, and friction wear behavior of iron aluminide coatings sprayed by HVOF. *J. Therm. Spray Technol.* 17:762–73
161. Amiriyani M, Alamdari HD, Blais C, Savoie S, Schulz R, Gariépy M. 2015. Dry sliding wear behavior of Fe<sub>3</sub>Al and Fe<sub>3</sub>Al/TiC coatings prepared by HVOF. *Wear* 342–343:154–62
162. Zhou Y, Wang SQ, Zhang BG, Zhang QY, Zhou DQ. 2017. Relation between tribolayers and wear behavior during dry sliding of Fe-Al hot-dipped coating. *Tribol. Trans.* 60:1078–87
163. Subramanian R, Schneibel JH. 1997. Processing iron-aluminide composites containing carbides or borides. *JOM* 49:50–54
164. Mosbah AY, Wexler D, Calka A. 2005. Abrasive wear of WC–FeAl composites. *Wear* 258:1337–41
165. Tu JP, Meng L, Liu MS. 1998. Friction and wear behavior of Cu-Fe<sub>3</sub>Al powder metallurgical composites in dry sliding. *Wear* 220:72–79
166. Velasco F, da Costa CE, Torralba JM. 2013. Mechanical properties and wear behaviour of PM aluminium composite reinforced with (Fe<sub>3</sub>Al) particles. *Powder Metall.* 45:247–50
167. Hawk JA, Alman DE. 1997. Abrasive wear of intermetallic-based alloys and composites. *Mater. Sci. Eng. A* 239–240:899–906
168. Alman DE, Hawk JA, Tylcak JH, Dogan CP, Wilson RD. 2001. Wear of iron–aluminide intermetallic-based alloys and composites by hard particles. *Wear* 251:875–84
169. Xia J, Li CX, Dong H. 2005. Thermal oxidation treatment of B2 iron aluminide for improved wear resistance. *Wear* 258:1804–12
170. Nowak K, Kupka M, Maszybrocka J, Barylski A. 2015. Effect of thermal oxidation process on wear resistance of B2 iron aluminide. *Vacuum* 114:221–25
171. Sharma G, Sundararaman M, Prabhu N, Goswami GL. 2003. Sliding wear resistance of iron aluminides. *Bull. Mater. Sci.* 26:311–14
172. Zhang X, Ma J, Fu L, Zhu S, Li F, et al. 2013. High temperature wear resistance of Fe–28Al–5Cr alloy and its composites reinforced by TiC. *Tribol. Int.* 61:48–55
173. Itoi T, Mineta S, Kinmura H, Yoshimi K, Hirohashi M. 2010. Fabrication and wear properties of Fe<sub>3</sub>Al-based composites. *Intermetallics* 18:2169–77
174. Tu JP, Liu MS. 1997. Wet abrasive wear of ordered Fe<sub>3</sub>Al alloys. *Wear* 209:31–36
175. Kim YS, Song JH, Chang YW. 1997. Erosion behavior of Fe-Al intermetallic alloys. *Scr. Mater.* 36:829–34
176. Tamann G, Siebel G. 1925. Die Anlauffarben auf Eisen-Kohlenstofflegierungen und auf Eisenmischkristallen: Fe-Ni; Fe-V; Fe-Al [Tarnish colors on iron-carbon alloys and iron solid solutions: Fe-Ni; Fe-V; Fe-Al]. *Z. Anorg. Allg. Chem.* 148:297–312
177. Hauttmann A. 1931. Hitzebeständigkeit von Aluminiumstählen und von Aluminiumüberzügen auf Eisen [Heat resistance of aluminum steels and aluminum coatings on iron]. *Stahl Eisen* 51:65–67

178. Sykes C, Bampfyld JW. 1934. The physical properties of iron-aluminium alloys. *J. Iron Steel Inst.* 130:389–418
179. Tomaszewicz P, Wallwork G. 1978. Iron-aluminium alloys: a review of their oxidation behaviour. *Rev. High Temp. Mater.* 4:75–104
180. Marx V, Palm M. 2017. Oxidation of Fe-Al alloys (5–40 at.% Al) at 700 and 900°C. *Mater. Sci. Forum* 879:1245–50
181. Prescott R, Graham MJ. 1992. The oxidation of iron-aluminum alloys. *Oxid. Met.* 38:73–87
182. Stumpf HC, Russell AS, Newsome JW, Tucker CM. 1950. Thermal transformations of aluminas and alumina hydrates. *Ind. Eng. Chem.* 42:1398–403
183. Wefers K, Misra C. 1987. *Oxides and Hydroxides of Aluminum*. Pittsburgh, PA: Alum. Co. Am.
184. Grabke HJ. 1999. Oxidation of NiAl and FeAl. *Intermetallics* 7:1153–58
185. Rommerskirchen I. 1996. *Oxidationsverhalten von  $\beta$ -NiAl und  $\beta$ -FeAl sowie Fe-Al-Legierungen [Oxidation behavior of  $\beta$ -NiAl,  $\beta$ -FeAl and Fe-Al alloys]*. Düsseldorf, Ger.: Fortschritt-Berichte VDI Verlag. 93 pp.
186. Das D, Balasubramaniam R, Mungole MN. 2002. Hot corrosion of Fe<sub>3</sub>Al. *J. Mater. Sci.* 37:1135–42
187. Lang F, Yu Z, Gedevanishvili S, Deevi SC, Narita T. 2003. Isothermal oxidation behavior of a sheet alloy of Fe-40at.% Al at temperatures between 1073 and 1473 K. *Intermetallics* 11:697–705
188. Lee DB, Kim GY, Kim JG. 2003. The oxidation of Fe<sub>3</sub>Al-(0, 2, 4, 6%)Cr alloys at 1000°C. *Mater. Sci. Eng. A* 339:109–14
189. Godlewska E. 2006. Effect of molybdenum on high-temperature corrosion of Fe-Al intermetallics. *Intermetallics* 14:280–86
190. Klöwer J, Li J-G. 1996. Effects of yttrium on the oxidation behaviour of iron-chromium-aluminium alloys. *Mater. Corros.* 47:545–51
191. Kim I, Cho WD, Kim HJ. 2000. High-temperature oxidation of Fe<sub>3</sub>Al containing yttrium. *J. Mater. Sci.* 35:4695–703
192. Natesan K. 1998. Corrosion performance of iron aluminides in mixed-oxidant environments. *Mater. Sci. Eng. A* 258:126–34
193. Pint BA, Schneibel JH. 2005. The effect of carbon and reactive element dopants on oxidation lifetime of FeAl. *Scr. Mater.* 52:1199–204
194. Pint BA, Wright IG. 2004. The oxidation behavior of Fe-Al alloys. *Mater. Sci. Forum* 461–464:799–806
195. Vogel D, Hotař A, Vogel A, Palm M, Renner FU. 2010. Corrosion behaviour of Fe-Al(-Ti) alloys in steam. *Intermetallics* 18:1375–78
196. Chevalier S, Juzon P, Przybylski K, Larpin JP. 2009. Water vapor effect on high-temperature oxidation behavior of Fe<sub>3</sub>Al intermetallics. *Sci. Technol. Adv. Mater.* 10:045006
197. Zhang Y, Pint BA, Haynes JA, Tortorelli PE. 2004. The effect of water vapor on the oxidation behavior of CVD iron-aluminide coatings. *Oxid. Met.* 62:103–20
198. Agüero A, Muelas R, Pastor A, Osgerby S. 2005. Long exposure steam oxidation testing and mechanical properties of slurry aluminide coatings for steam turbine components. *Surf. Coat. Technol.* 200:1219–24
199. Sánchez L, Bolívar FJ, Hierro MP, Pérez FJ. 2008. Effect of Ce and La additions in low temperature aluminization process by CVD-FBR on 12%Cr ferritic/martensitic steel and behaviour in steam oxidation. *Corros. Sci.* 50:2318–26
200. Judkins RR, Rao US. 2000. Fossil energy applications of intermetallic alloys. *Intermetallics* 8:1347–54
201. DeVan JH, Tortorelli PF. 1993. The oxidation-sulfidation behavior of iron alloys containing 16–40 at.% aluminum. *Corros. Sci.* 35:1065–71
202. Kai W, Douglass DL. 1993. The high-temperature corrosion behavior of Fe-Mo-Al alloys in H<sub>2</sub>/H<sub>2</sub>O/H<sub>2</sub>S mixed-gas environments. *Oxid. Met.* 39:281–316
203. Klöwer J. 1996. High-temperature corrosion behavior of iron aluminides and iron-aluminum-chromium alloys. *Mater. Corros.* 47:685–94
204. Tortorelli PF, DeVan JH. 1992. Behavior of iron aluminides in oxidizing and oxidizing/sulfidizing environments. *Mater. Sci. Eng. A* 153:573–77
205. Stott FH, Chuah KT, Bradley LB. 1996. Oxidation-sulphidation of iron aluminides at high temperature. *Mater. Corros.* 47:695–700

206. Ilyushechkin AY, Dolan MD, McLennan KG, Sharma SD. 2011. Effect of pre-oxidation of Fe<sub>3</sub>Al on its corrosion resistance in sulfur and chlorine contaminated syngas. *Asia Pac. J. Chem. Eng.* 7:716–25
207. Strauß S, Krajak R, Palm M, Grabke HJ. 1996. Metal dusting of Fe<sub>3</sub>Al and (Fe,Ni)<sub>3</sub>Al. *Mater. Corros.* 47:701–2
208. Bernst R, Schneider A, Spiegel M. 2006. Metal dusting of binary iron aluminium alloys at 600°C. *Mater. Corros.* 57:724–28
209. Schneider A, Zhang J. 2003. Metal dusting of ferritic Fe-Al-M-C (M = Ti, V, Nb, Ta) alloys in CO-H<sub>2</sub>-H<sub>2</sub>O gas mixtures at 650°C. *Mater. Corros.* 54:778–84
210. Schneider A, Zhang J, Inden G. 2004. Metal dusting of binary Fe-Al alloys in CO-H<sub>2</sub>-H<sub>2</sub>O gas mixtures. *J. Corros. Sci. Eng.* 6:87
211. Duquette DJ. 1995. Corrosion of intermetallic compounds. See Ref 299, pp. 965–75
212. Morris DG, Muñoz-Morris MA. 2011. Recent developments toward the application of iron aluminides in fossil fuel technologies. *Adv. Eng. Mater.* 13:43–47
213. Rao VS. 2004. A review of the electrochemical corrosion behaviour of iron aluminides. *Electrochim. Acta* 49:4533–42
214. Madsen BW, Adler TA. 1994. Passivation and repassivation kinetics of iron-aluminum alloys in 1 N H<sub>2</sub>SO<sub>4</sub> using potential step and scratch tests. *Wear* 171:215–25
215. Kim JG, Buchanan RA. 1994. Pitting and crevice corrosion of iron aluminides in a mild acid-chloride solution. *Corrosion* 50:658–68
216. Choe HC, Kim HS, Choi DC, Kim KH. 1997. Effects of alloying elements on the electrochemical characteristics of iron aluminides. *J. Mater. Sci.* 32:1221–27
217. Peng J, Moszner F, Rechmann J, Vogel D, Palm M, Rohwerder M. 2019. Influence of Al content and pre-oxidation on the aqueous corrosion resistance of binary Fe-Al alloys in sulphuric acid. *Corros. Sci.* 149:123–32
218. Buchanan RA, Perrin RL. 1997. Effects of 1000°C oxide surfaces on room temperature aqueous corrosion and environmental embrittlement of iron aluminides. In *11th Annual Conference on Fossil Energy Materials*, ed. RR Judkins, pp. 159–68. Oak Ridge, TN: Oak Ridge Natl. Lab.
219. Lopez MF, Escudero ML. 1998. Corrosion behaviour of FeAl-type intermetallic compounds. *Electrochim. Acta* 43:671–78
220. Escudero ML, García-Alonso MC, González-Carrasco JL, Muñoz-Morris MA, Montealegre MA, et al. 2003. Possibilities for improving the corrosion resistance of Fe-40Al intermetallic strip by prior oxide protection. *Scr. Mater.* 48:1549–54
221. Masahashi N, Kimura G, Oku M, Konmatsu K, Watanabe S, Hanada S. 2006. Corrosion behavior of iron-aluminium alloys and its composite steel in sulfuric acid. *Corros. Sci.* 48:829–39
222. Palm M, Krieg R. 2012. Neutral salt spray tests on Fe-Al and Fe-Al-X. *Corros. Sci.* 64:74–81
223. Maziasz PJ, Goodwin GM, Alexander DJ, Viswanathan S. 1997. Alloy development and processing effects for FeAl iron aluminides: an overview. In *International Symposium on Nickel and Iron Aluminides: Processing, Properties, and Applications*, ed. SC Deevi, PJ Maziasz, VK Sikka, RW Cahn, pp. 157–76. Materials Park, OH: ASM Int.
224. Tortorelli PE, Bishop PS. 1991. *Influence of compositional modifications on the corrosion of iron aluminides by molten nitrate salts*. Rep. ORNL/TM-11598, Oak Ridge Natl. Lab., Oak Ridge, TN
225. Frangini S. 2000. Corrosion behavior of AISI 316L stainless steel and ODS FeAl aluminate in eutectic Li<sub>2</sub>CO<sub>3</sub>-K<sub>2</sub>CO<sub>3</sub> molten carbonates under flowing CO<sub>2</sub>-O<sub>2</sub> gas mixtures. *Oxid. Met.* 53:139–56
226. Amaya M, Espinosa-Medina MA, Porcayo-Calderon J, Martinez L, Gonzalez-Rodriguez JG. 2003. High temperature corrosion performance of FeAl intermetallic alloys in molten salts. *Mater. Sci. Eng. A* 349:12–19
227. Huang YD, Yang WY, Sun ZQ, Froyen L. 2004. Preparation and mechanical properties of large-ingot Fe<sub>3</sub>Al-based alloys. *J. Mater. Proc. Technol.* 146:175–80
228. Sikka VK, Wilkening D, Liebetrau J, Mackey B. 1998. Melting and casting of FeAl-based alloy. *Mater. Sci. Eng. A* 258:229–35
229. Kettner U, Rehfeld H, Engelke C, Neuhäuser H. 1999. A comparison of the plastic behaviour of Fe<sub>3</sub>Al and Fe<sub>3</sub>Si in the temperature range of 300–973 K. *Intermetallics* 7:405–14

230. Yasuda HY, Nakano K, Nakajima T, Ueda M, Umakoshi Y. 2003. Effect of ordering process on giant pseudoelasticity in Fe<sub>3</sub>Al single crystals. *Acta Mater.* 51:5101–12
231. Radhakrishna A, Baligidad RG, Sarma DS. 2001. Effect of carbon on structure and properties of FeAl based intermetallic alloy. *Scr. Mater.* 45:1077–82
232. Itoi T, Watanabe Y, Nishikawa Y, Kimura H, Yoshimi K, Hirohashi M. 2010. Preparation of recycle-typed Fe<sub>3</sub>Al alloy and its application for cutting tool materials. *Intermetallics* 18:1396–400
233. Borges DFL, Espinosa DCR, Schön CG. 2014. Making iron aluminides out of scrap. *J. Mater. Res. Technol.* 3:101–6
234. Rabin BH, Wright RN. 1991. Synthesis of iron aluminides from elemental powders: reaction mechanisms and densification behavior. *Metal. Trans.* 22A:277–86
235. Wright RN, Rabin BH, Wright JK. 1993. *Processing, properties, and wear resistance of aluminides*. Rep. EGG-MS-10441, Idaho Natl. Eng. Lab., Idaho Falls, ID
236. Godlewska E, Szczepanik S, Mania R, Krawiarz J, Kozinski S. 2003. FeAl materials from intermetallic powders. *Intermetallics* 11:307–12
237. Novák P, Knotek V, Serák J, Michalcová A, Vojtech D. 2011. Synthesis of Fe–Al–Si intermediary phases by reactive sintering. *Powder Metall.* 54:167–71
238. Matsumoto A, Kobayashi K, Nishio T, Ozaki K, Sugiyama A. 2000. Microstructure and mechanical properties of FeAl compacts prepared by pulse current sintering of mechanically alloyed powders. *J. Jpn. Soc. Powder Powder Metall.* 47:1253–57
239. Paris S, Gaffet E, Bernard F, Munir ZA. 2004. Spark plasma synthesis from mechanically activated powders: a versatile route for producing dense nanostructured iron aluminides. *Scr. Mater.* 50:691–96
240. Deevi SC, Sikka VK. 1997. Reaction synthesis and processing of nickel and iron aluminides. In *International Symposium on Nickel and Iron Aluminides: Processing, Properties, and Applications*, ed. SC Deevi, PJ Maziasz, VK Sikka, RW Cahn, pp. 283–99. Materials Park, OH: ASM Int.
241. Liu CT, Sikka VK, McKamey CG. 1993. *Alloy development of FeAl aluminide alloys for structural use in corrosive environments*. Rep. ORNL/TM-12199, Oak Ridge Natl. Lab., Oak Ridge, TN
242. Testani C, Di Gianfrancesco A, Tassa O, Pocci D. 1997. FeAl intermetallics and applications: an overview. In *International Symposium on Nickel and Iron Aluminides: Processing, Properties, and Applications*, ed. SC Deevi, PJ Maziasz, VK Sikka, RW Cahn, pp. 213–22. Materials Park, OH: ASM Int.
243. McQuay PA, Sikka VK. 2002. Casting. See Ref 301, pp. 591–616
244. Blackford JR, Buckley RA, Jones H, Sellars CM. 1996. Production of iron aluminides by strip casting followed by cold rolling at room temperature. *Scr. Mater.* 34:1595–600
245. Flores O, Juarez J, Campillo B, Martinez L, Schneibel JH. 1994. Forging of FeAl intermetallic compounds. See Ref 303, pp. 31–38
246. Rodriguez J, Moussa SO, Wall J, Morsi K. 2003. Low-energy forging of aluminide intermetallics. *Scr. Mater.* 48:707–12
247. Yu XQ, Sun YS. 2004. Hot working of Fe<sub>3</sub>Al based alloy. *Mater. Sci. Technol.* 20:339–42
248. Morris DG, Muñoz-Morris MA. 2010. High creep strength, dispersion-strengthened iron aluminide prepared by multidirectional high-strain forging. *Acta Mater.* 58:6080–89
249. Zhang ZH, Sun YS, Shen GJ. 1998. Improvements of tensile strength and creep resistance of Fe-28Al alloy with tungsten addition. *Scr. Mater.* 38:21–25
250. Huang YD, Yang WY, Sun ZQ. 1999. Improvement of room temperature tensile properties for Fe<sub>3</sub>Al-based alloys by thermomechanical and annealing processes. *Mater. Sci. Eng. A* 263:75–84
251. Janschek P, Bauer-Partenheimer K, Krein R, Hanus P, Palm M. 2009. Forging of steam turbine blades with an Fe<sub>3</sub>Al-based alloy. *Mater. Res. Soc. Symp. Proc.* 1128:47–52
252. Palm M, Stein F, Dehm G. 2017. Entwicklung intermetallischer Eisenaluminid-Legierungen [Development of intermetallic iron aluminide alloys]. *Stahl Eisen* 137:76
253. Blackford JR, Buckley RA, Jones H, Sellars CM, Briguet C, Morris DG. 1998. Effect of process variables on tensile properties of ingot processed versus strip cast iron aluminides. *Mater. Sci. Technol.* 14:1132–38
254. Deevi SC, Sastry DH, Sikka VK. 2001. Alloy development and industrial processing of iron aluminide sheets. In *Structural Intermetallics 2001*, ed. KJ Hemker, DM Dimiduk, H Clemens, R Darolia, H Inui, et al., pp. 111–19. Warrendale, PA: TMS

255. Baligheid RG, Radhakrishna A. 2004. Effect of zirconium on structure and properties of high carbon Fe–10.5 wt-% Al alloy. *Mater. Sci. Technol.* 20:111–16
256. Kratochvil P, Schindler I, Hanus P. 2006. Conditions for the hot rolling of Fe<sub>3</sub>Al-type iron aluminide. *Koovo Mater.* 44:321–26
257. Kuc D, Niewielski G, Bednarczyk I. 2008. The influence of thermomechanical treatment on structure of FeAl intermetallic phase-based alloys. *JAMME* 29:123–30
258. Schindler I, Kratochvil P, Prokopcakova P, Kozelsky P. 2010. Forming of cast Fe–45 at.% Al alloy with high content of carbon. *Intermetallics* 18:745–47
259. Huang YD, Yang WY, Chen GL, Sun ZQ. 2001. On the effect of the B2 thermomechanical treatment in improving the room temperature ductility of Fe<sub>3</sub>Al-based alloys. *Intermetallics* 9:331–40
260. Deevi SC, Hajaligol MR, Sikka VK, McKernon J, Scorey CR. 1999. Processing and properties of FeAl sheets obtained by roll compaction and sintering of water atomized powders. *Mater. Res. Soc. Symp. Proc.* 552:KK4.6.1
261. Seetharaman V, Semiatin SL. 2002. Powder metallurgy. See Ref 301, pp. 643–62
262. Strothers S, Vedula K. 1987. Hot extrusion of B2 iron aluminide powders. *Prog. Powder Metall.* 43:597–610
263. Sikka VK, Viswanathan S, McKamey CG. 1993. Development and commercialization status of Fe<sub>3</sub>Al-based intermetallic alloys. In *Structural Intermetallics*, ed. R Darolia, JJ Lewandowski, CT Liu, PL Martin, DB Miracle, MV Nathal, pp. 483–91. Warrendale, PA: TMS
264. Kad B, Heatherington H, McKamey CG, Wright IG, Sikka VK, Judkins RR. 2003. Optimization of high temperature hoop creep response in ODS-Fe<sub>3</sub>Al tubes. In *17th Annual Conference on Fossil Energy Materials*, ed. RR Judkins, pp. 1–10. Baltimore, MD: US Dep. Energy Off. Sci. Tech. Inf.
265. Durejko T, Lipinski S, Bojar Z, Bystrzycki J. 2011. Processing and characterization of graded metal/intermetallic materials: the example of Fe/FeAl intermetallics. *Mater. Des.* 32:2827–34
266. Song B, Dong S, Coddet P, Liao H, Coddet C. 2012. Fabrication and microstructure characterization of selective laser-melted FeAl intermetallic parts. *Surf. Coat. Technol.* 206:4704–9
267. Durejko T, Zietala M, Polkowski W, Czujko T. 2014. Thin wall tubes with Fe<sub>3</sub>Al/SS316L graded structure obtained by using laser engineered net shaping technology. *Mater. Des.* 63:766–74
268. Cinca N, Guilemany JM. 2012. Thermal spraying of transition metal aluminides: an overview. *Intermetallics* 24:60–72
269. Cinca N, Lima CRC, Guilemany JM. 2013. An overview of intermetallics research and application: status of thermal spray coatings. *J. Mater. Res. Technol.* 2:75–86
270. Datta PK, Burnell-Gray JS, Natesan K. 2002. Coating technology. See Ref 301, pp. 561–88
271. Sikka VK, Swindeman RW, Wright IG, Judkins RR, Johnson R. 1999. Fabrication of test tubes for coal ash corrosion testing. In *13th Conference on Fossil Energy Materials*, pp. 1–17. Oak Ridge, TN: Oak Ridge Natl. Lab.
272. Sasaki T, Yakou T. 2006. Machinability of intermetallic compound Fe<sub>3</sub>Al from the view point of tool wear. *JSM Int. J. C* 49:334–39
273. Liu L, Shao H, Huang LX. 2009. Studies on drilling processes of intermetallic compounds. *J. Mater. Proc. Technol.* 209:4509–14
274. Köhler J, Moral A, Denkena B. 2013. Grinding of iron-aluminides. *Proc. CIRP* 9:2–7
275. Deneka B, Reichenstein M, Meyer R, Deges J. 2005. Machining of iron-aluminium-based alloys: wear behaviour of uncoated cemented carbide tools while turning an Fe<sub>3</sub>Al-based alloy. *wt-online* 11/12-2005:910–14
276. David SA, Horton JA, McKamey CG, Zacharia T, Reed RW. 1989. Welding of iron aluminides. *Welding J.* 68:s372–81
277. Santella ML. 1997. An overview of the welding of Ni<sub>3</sub>Al and Fe<sub>3</sub>Al alloys. In *International Symposium on Nickel and Iron Aluminides: Processing, Properties, and Applications*, ed. SC Deevi, PJ Maziasz, VK Sikka, RW Cahn, pp. 321–27. Materials Park, OH: ASM Int.
278. McKamey CG, Maziasz PJ, Goodwin GM, Zacharia T. 1994. Effects of alloying additions on the microstructures, mechanical properties and weldability of Fe<sub>3</sub>Al-based alloys. *Mater. Sci. Eng. A* 174:59–70

279. Sketchley PD, Threadgill PL, Wright IG. 2002. Rotary friction welding of an Fe<sub>3</sub>Al based ODS alloy. *Mater. Sci. Eng. A* 329–331:756–62
280. Chiang CC, Wang SH, Chen JS, Chu JP, Hsu YF. 2007. Bending embrittlement of as-welded FeAl alloys. *Intermetallics* 15:564–70
281. Neumann H, Moravec J, Bradac J. 2010. TIG welding process effect on the iron aluminide Fe<sub>3</sub>Al. In *METAL 2010*, pp. 1–6. Ostrava, Czech Rep.: Tanger
282. Cebulski J. 2015. Application of FeAl intermetallic phase matrix based alloys in the turbine components of a turbo charger. *Metallurgija* 54:154–56
283. Blau PJ, Meyer HM III. 2003. Characteristics of wear particles produced during friction tests of conventional and unconventional disc brake materials. *Wear* 255:1261–69
284. Tyszko Z. 1969. Fontes a haute teneur en aluminium [Cast iron with high content in aluminum]. *Fonderie* 278:221–33
285. Xiang X, Wang X, Zhang G, Tang T, Lai X. 2015. Preparation technique and alloying effect of aluminide coatings as tritium permeation barriers: a review. *Int. J. Hydrogen Energ.* 40:3697–707
286. Sikka VK, Blue CA, Sklad SP, Deevi SC, Shih H-R. 1998. Fabric cutting application of FeAl-based alloys. *Mater. Sci. Eng. A* 256:325–30
287. Landis GA. 2007. Materials refining on the moon. *Acta Astronaut.* 60:906–15
288. McKamey CG, McCleary D, Tortorelli PF, Sawyer J, Lara-Curzio E, Judkins RR. 2002. Characterization of field-exposed iron aluminide hot gas filters. In *Proceedings of the 5th International Symposium on Gas Cleaning at High Temperature*, pp. 1–15. Morgantown, WV: Natl. Energy Technol. Lab.
289. Pall Corporation. 2018. *S series PSS<sup>®</sup> filter elements*. Datasheet E20c. <https://shop.pall.com/us/en/oil-gas/refinery/refinery-react/catalyst-protect-/s-series-pss-filter-elements-zidgri78lfx>
290. Zhang H, Liu X, Jiang Y, Gao L, Yu L, et al. 2017. Direct separation of arsenic and antimony oxides by high-temperature filtration with porous FeAl intermetallic. *J. Hazard. Mater.* 338:364–71
291. Schulz R, Savoie S. 2009. A new family of high performance nanostructured catalysts for the electrosynthesis of sodium chlorate. *J. Alloys Compd.* 483:510–13
292. Armbrüster M, Kovnir K, Friedrich M, Teschner D, Wowsnick G, et al. 2012. Al<sub>13</sub>Fe<sub>4</sub> as a low-cost alternative for palladium in heterogeneous hydrogenation. *Nature Mater.* 11:690–93
293. Herrmann J. 2000. *Untersuchungen zur Struktur und zum mechanischen Verhalten von Fe-reichen Fe-Al-Legierungen [Investigations concerning the structure and mechanical behavior of Fe-rich Fe-Al alloys]*. Doctoral Thesis, RWTH Aachen. 167 pp.
294. Herrmann J, Inden G, Sauthoff G. 2003. Deformation behaviour of iron-rich iron-aluminium alloys at low temperatures. *Acta Mater.* 51:2847–57
295. Eumann M, Palm M, Sauthoff G. 2004. Alloys based on Fe<sub>3</sub>Al or FeAl with strengthening Mo<sub>3</sub>Al precipitates. *Intermetallics* 12:625–33
296. Sundar RS, Kutty TRG, Sastry DH. 2000. Hot hardness and creep of Fe<sub>3</sub>Al-based alloys. *Intermetallics* 8:427–37
297. Knezevic V, Sauthoff G, Vilk J, Inden G, Schneider A, et al. 2002. Martensitic/ferritic super heat-resistant 650°C steels: design and testing of model alloys. *ISIJ Int.* 42:1505–14
298. Palm M, Krein R, Milenkovic S, Sauthoff G, Risanti D, et al. 2007. Strengthening mechanisms for Fe-Al-based alloys with increased creep resistance at high temperatures. *Mater. Res. Soc. Symp. Proc.* 980:II01
299. Westbrook JH, Fleischer RL, ed. 1995. *Intermetallic Compounds: Principles and Practice. Vol. 1: Principles*. Chichester, UK: John Wiley & Sons
300. Westbrook JH, Fleischer RL, ed. 1995. *Intermetallic Compounds: Principles and Practice. Vol. 2: Practice*. Chichester, UK: John Wiley & Sons
301. Westbrook JH, Fleischer RL, ed. 2002. *Intermetallic Compounds: Principles and Practice. Vol. 3: Progress*. Chichester, UK: John Wiley & Sons
302. Stoloff NS, Sikka VK, ed. 1996. *Physical Metallurgy and Processing of Intermetallic Compounds*. Boston, MA: Springer US
303. Schneibel JH, Crimp MA, ed. 1994. *Processing, Properties, and Applications of Iron Aluminides*. Warrendale, PA: TMS

# Contents

## Computational Methods in Materials

Advances in Density-Functional Calculations for Materials Modeling <i>Reinhard J. Maurer, Christoph Freysoldt, Anthony M. Reilly, Jan Gerit Brandenburg, Oliver T. Hofmann, Torbjörn Björkman, Sébastien Lebègue, and Alexandre Tkatchenko</i> .....	1
Applications of DFT + DMFT in Materials Science <i>Arpita Paul and Turan Birol</i> .....	31
Modeling Corrosion with First-Principles Electrochemical Phase Diagrams <i>Liang-Feng Huang, John R. Scully, and James M. Rondinelli</i> .....	53
The Phase Field Method: Mesoscale Simulation Aiding Material Discovery <i>Michael R. Tonks and Larry K. Aagesen</i> .....	79
Systems Approaches to Materials Design: Past, Present, and Future <i>Raymundo Arróyave and David L. McDowell</i> .....	103
Understanding, Predicting, and Designing Ferroelectric Domain Structures and Switching Guided by the Phase-Field Method <i>Jian-Jun Wang, Bo Wang, and Long-Qing Chen</i> .....	127

## Topological Quantum Materials

Topological Semimetals from First Principles <i>Heng Gao, Jörn W.F. Venderbos, Youngkuk Kim, and Andrew M. Rappe</i> .....	153
Topological Semimetals in Square-Net Materials <i>Sebastian Klemenz, Shiming Lei, and Leslie M. Schoop</i> .....	185
Transport of Topological Semimetals <i>Jin Hu, Su-Yang Xu, Ni Ni, and Zhiqiang Mao</i> .....	207

## Current Interest

Challenges of the Circular Economy: A Material, Metallurgical, and Product Design Perspective <i>Markus A. Reuter, Antoinette van Schaik, Jens Gutzmer, Neill Bartie, and Alejandro Abadías-Llamas</i> .....	253
Cold Sintering: Progress, Challenges, and Future Opportunities <i>Jing Guo, Richard Floyd, Sarah Lowum, Jon-Paul Maria, Thomas Herisson de Beauvoir, Joo-Hwan Seo, and Clive A. Randall</i> .....	275
Iron Aluminides <i>Martin Palm, Frank Stein, and Gerhard Dehm</i> .....	297
Materials for Automotive Lightweighting <i>Alan Taub, Emmanuel De Moor, Alan Luo, David K. Matlock, John G. Speer, and Uday Vaidya</i> .....	327
Mechanical Control of Magnetic Order: From Phase Transition to Skyrmions <i>Jie Wang</i> .....	361
Time-Resolved X-Ray Microscopy for Materials Science <i>Haidan Wen, Mathew J. Cherukara, and Martin V. Holt</i> .....	389

## Indexes

Cumulative Index of Contributing Authors, Volumes 45–49 .....	417
---	-----

## Errata

An online log of corrections to *Annual Review of Materials Research* articles may be found at <http://www.annualreviews.org/errata/matsci>